MAR Neurology, Neurosurgery & Psychology (2024) 8:4
Research Article

Targeting Glioblastoma: Inducing Necroptosis molecular pathway Post- Photodynamic Therapy for Enhanced Neurosurgical and Therapeutic Outcomes

Nazar Vasyliv *

***Correspondence to:** Nazar Vasyliv, University of Edinburgh, MD, MSc Precision Oncology & Cancer Research, PhD candidate, Centre for Clinical Brain Sciences, Edinburgh, Chancellor's Building 49 Little France Crescent, EH16 4SB, University of Glasgow affiliate, Wolfson Wohl Cancer Research Centre, Institute of Cancer Sciences, Beatson Institute for Cancer Research affiliate, Garscube Estate, Glasgow, UK, G61 1QH. CEO, Global Alliance for Neurosurgical & Brain Cancer Research Innovations.

Email**: N. Vasyliv@sms.ed.ac.uk**

Copyright

Received: 01 September 2024

Published: 20 September 2024

Abstract

Glioblastoma (GBM) remains a formidable challenge in neurosurgery and oncology due to its aggressive progression and resistance to standard therapies. This study investigates the potential of enhancing photodynamic therapy (PDT) efficacy by inducing necroptosis—a regulated form of necrotic cell death—in glioblastoma stem cells (GSCs). We hypothesize that combining PDT with necroptosis induction could overcome the limitations of conventional approaches by targeting resistant tumor cell populations, ultimately improving clinical outcomes. This work provides insights into the molecular mechanisms underlying this combinatorial strategy and its potential translational impact in GBM treatment.

Acknowledgments

I wish to express my profound gratitude to Dr. Karin Williams, PhD, at the University of Glasgow and the WWCRC, for her exceptional mentorship throughout the course of my research. Her insightful guidance, constructive feedback, and unwavering support have been integral to the development and success of this work. Dr. Williams' expertise and dedication to fostering a collaborative and intellectually stimulating environment have significantly influenced my academic journey.

I am also deeply indebted to Dr. Kirsteen Campbell, PhD, at the Beatson Cancer Institute, University of Glasgow, for her invaluable feedback and personal support. Dr. Campbell's encouragement, astute insights, and thoughtful advice have been instrumental in shaping both my research and my personal growth. Her commitment to excellence has left a lasting impact on my professional and personal life.

Furthermore, I would like to extend my heartfelt thanks to Emeritus Professor Bertil Rydenhag, University of Gothenburg, Sweden, for his meticulous proofreading of this manuscript and its references. His keen eye for detail and thorough review have greatly enhanced the quality and clarity of this work. I am also deeply appreciative of the valuable advice and guidance he provided throughout this process. Professor Rydenhag's expertise and thoughtful suggestions have been instrumental in refining this research, and I am truly grateful for his generous support.

I would also like to express my sincere gratitude to the Beatson Cancer Charity for their financial support, which made this research possible. Their commitment to funding critical cancer research has been vital to the progress of this work and is deeply appreciated.

I am honored to acknowledge the creation of the Global Alliance for Neurosurgical and Brain Cancer Research, a non-profit organization dedicated to providing invaluable support to those suffering from brain cancer. Led by Nazar Vasyliv (CEO) and Oleksandr Tverdokhlib (CFO), this organization will foster professional partnerships and unite leaders across the world to advance research and offer critical assistance to patients and their families.

I would like to extend my heartfelt thanks to Dr. Akhill Kallepalli, the University of Strathclyde, Department of Biomedical Engineering, and the School of Physics and Astronomy at the University of Glasgow, including Graham Gibson and Prof. Miles Padgett, for their significant contributions. The additional photodynamic therapy rigs, generously provided through their collaborative efforts, have been instrumental in advancing our work. I am deeply grateful for their generosity and unwavering commitment to our shared goals.

Finally, I would like to acknowledge that the process of completing this research has been enriched by a range of perspectives and experiences. The collaborative efforts and insights gained from working across various institutions have been invaluable, contributing significantly to my development as a researcher and shaping the direction of this work in meaningful ways.

Introduction

Glioblastoma (GBM) is the most aggressive and lethal primary brain tumor in adults, distinguished by rapid proliferation, extensive infiltration into surrounding neural tissue, and a highly heterogeneous cellular composition **[**1**]**. Despite advances in surgical techniques, radiation therapy, and chemotherapy, the median survival for GBM patients remains just 15 months **[**2**]**. The tumor's invasive nature and its tendency to involve critical brain structures make complete surgical resection challenging, leading to persistently high recurrence rates **[**3**]**.

Photodynamic therapy (PDT), which utilizes photosensitizers such as 5-aminolevulinic acid (5-ALA), offers a targeted approach designed to exploit the metabolic vulnerabilities of GBM cells **[**4**]**. 5-ALA is selectively absorbed by tumor cells and metabolized into protoporphyrin IX (PpIX), a potent photosensitizer. When activated by specific wavelengths of light, PpIX generates reactive oxygen species (ROS) that induce oxidative stress and cellular damage within the tumor **[**5**]**. Recent studies suggest that enhancing PDT with molecular strategies to induce necroptosis—a regulated form of necrotic cell death—could significantly improve therapeutic efficacy by overcoming the apoptotic resistance often observed in GBM **[**6**]**.

Challenges in Neurosurgical Resection and PDT Penetration

The primary goal of neurosurgical resection in GBM management is to maximize tumor debulking while preserving essential neurological function **[**7**]**. However, the highly infiltrative nature of GBM often results in residual microscopic disease that evades detection and removal during surgery **[**8**]**. While PDT is effective in targeting superficial tumor remnants, its limited penetration depth into brain tissue constrains its ability to eliminate deeper tumor deposits **[**9**]**. The ROS generated by PDT are confined to regions of light exposure, leaving deeper, non-illuminated tumor cells unaffected, contributing to eventual disease recurrence **[**10**]**.

These limitations highlight the need for combinatorial therapeutic strategies that can enhance treatment efficacy synergistically **[**11**]**. Residual GBM cells, often located in hypoxic and poorly vascularized regions of the tumor bed, show increased resistance to conventional therapies and contribute to tumor recurrence **[**12**]**. Therefore, combining PDT with necroptosis-inducing agents presents a promising approach to eradicating these residual, treatment-resistant cells, potentially improving patient outcomes **[**13**]**.

Photodynamic Therapy (PDT): Molecular Mechanisms and Clinical Applications

PDT leverages the altered metabolic landscape of GBM cells, where photosensitizers like 5- ALA are preferentially accumulated and converted into PpIX due to the upregulated heme biosynthesis pathway in tumor cells **[**14**]**. Upon exposure to light within PpIX's absorption spectrum (typically around 635 nm), the excited photosensitizer interacts with molecular oxygen to produce singlet oxygen and other ROS, initiating oxidative damage **[**15**]**. Traditionally, PDT-induced cell death has been attributed to apoptosis; however, recent findings suggest that PDT can also trigger necroptosis, especially when apoptotic pathways are impaired or blocked **[**16**]**.

Necroptosis is mediated by a signaling cascade involving receptor-interacting protein kinases 1 and 3 (RIPK1 and RIPK3) and the downstream effector, mixed lineage kinase domain-like protein (MLKL) **[**17**]**. Once phosphorylated, MLKL translocates to the plasma membrane, where it forms pores that compromise membrane integrity, leading to cell lysis and the release of damage-associated molecular patterns (DAMPs) **[**18**]**. This form of cell death is particularly beneficial in GBM, where resistance to apoptosis is common, offering an alternative pathway to ensure tumor cell elimination **[**17**]**.

Clinical Implications of Inducing Necroptosis Post-PDT

Inducing necroptosis following PDT is a promising strategy to enhance tumor cell death in GBM, particularly in cells resistant to apoptosis **[**19**]**. By targeting the RIPK1/RIPK3/ MLKL axis, necroptosis can be effectively triggered in residual tumor cells, amplifying the cytotoxic effects of PDT and reducing the likelihood of disease recurrence **[**20**]**. Clinical studies have shown that inhibiting key apoptotic regulators, such as caspase-8, can enhance necroptotic signaling in GBM cells post-PDT, thus improving therapeutic outcomes **[**21**]**. This dual-targeted approach—combining PDT with necroptosis induction—may be particularly effective in targeting the heterogeneous cell populations within GBM, including cancer stem cells that are typically resistant to conventional therapies **[**22**]**.

Moreover, clinical trials evaluating PDT's efficacy in GBM treatment have reported improvements in surgical resection margins and overall survival, especially when combined with 5-ALA as a fluorescence-guided surgical adjunct **[**23**]**. The phase III trial by Stummer et al. demonstrated the benefits of 5-ALA-guided resection in extending progression-free survival, further supporting the integration of PDT into

standard GBM treatment protocols [24]. Preclinical studies also suggest that combining PDT with necroptosis-inducing agents, such as RIPK3 agonists or MLKL activators, may further enhance this approach's therapeutic efficacy [25]. Continued clinical trials are crucial to validate these combinatorial strategies' safety and effectiveness in GBM patients [26].

The development of personalized treatment strategies, tailored to the molecular profile of individual tumors, will be vital for optimizing the therapeutic benefits of PDT combined with necroptosis induction [27]. Future research should focus on identifying biomarkers that predict responsiveness to PDT and necroptosis-based therapies, enabling the selection of patients most likely to benefit from these advanced treatments [28]. Ongoing and future clinical trials will be pivotal in translating these experimental findings into clinical practice, ultimately improving outcomes for patients with this challenging disease [29].

Historical Context of Photodynamic Therapy in GBM

Unlike chemotherapy and radiation therapy for GBM, the light used in photodynamic therapy has a low mutagenic effect [30]. The history of photodynamic therapy dates to 1903 when Finsen was awarded the Nobel Prize for his pioneering use of light in treating diseases, laying the foundation for PDT [31]. A decade later, Raab and Joblbauer, along with Von Tappeiner and Jesionick, discovered that acridine dyes could induce a photodynamic reaction, although these findings were not widely adopted until the discovery of 5-ALA, which found its place in GBM resections as a substrate for PDT [32].

5-ALA, a product of the heme degradation pathway, is currently used in fluorescence- guided surgery (FGS). PDT, therefore, is not only applied in the neurosurgical resection of GBM but is also widely utilized in research. PDT involves the interaction of a PS with light, typically within wavelengths ranging from 460 to 800 nm, leading to the generation of ROS and subsequent tumor cell death [33,34]. Various studies have proposed different wavelengths for targeting glioma cells, but there is no clear evidence that any specific wavelength consistently induces cell death in GBM cells. For instance, PDT with 5-ALA can produce blue illumination at 410 nm, green at 528 nm, and red at 635 nm, each affecting GBM cells differently. Despite extensive research, only a few photosensitizers have shown significant efficacy in clinical trials involving GBM patients, with varying side effects [35,36,37]. These photosensitizers have been tested in previous studies and have exhibited different side effects in patients undergoing FGS for GBM [38,39].

This study aims to unravel the intricate molecular mechanisms governing cell death in GSCs induced by

PDT with 5-ALA. We propose that PDT/5-ALA triggers cell death in GSCs through the activation of two distinct yet potentially interconnected molecular pathways: apoptosis and necroptosis. Our hypothesis is that PDT/5-ALA induces a dual- pathway response, where apoptosis and necroptosis are not merely parallel events but may interact through cross-regulatory networks that influence GSC viability.

PDT/5-ALA is hypothesized to induce apoptosis in GSCs via the mitochondrial pathway, characterized by cytochrome c release and subsequent activation of caspase-9 and caspase-3. This apoptotic cascade is likely modulated by Bcl-2 family proteins and p53, leading to cell death through programmed mechanisms. Concurrently, PDT/5-ALA is expected to activate necroptosis through receptor-interacting protein kinase 1 (RIPK1), RIPK3, and MLKL. We hypothesize that necroptosis may be triggered in GSCs when apoptosis is inhibited or overwhelmed, representing an alternative cell death pathway in response to PDT-induced stress. Our experimental approach will involve a comparative analysis of these pathways, using specific inhibitors to dissect their individual and interactive roles. We will assess key biomarkers and signaling intermediates involved in both apoptotic and necroptotic processes, as detailed in **Figure 1**. This investigation aims to uncover the molecular crosstalk between apoptosis and necroptosis in GSCs post-PDT/5- ALA and to elucidate how these pathways might converge or diverge in the context of glioblastoma treatment.

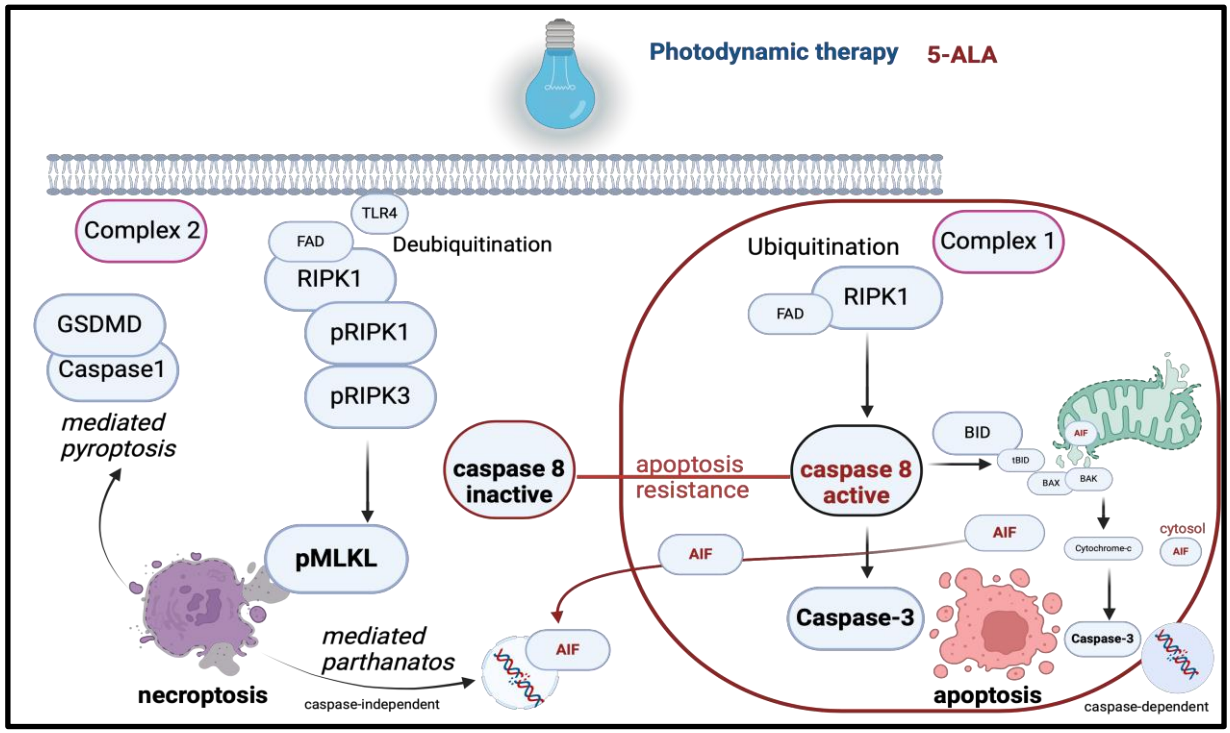

Fig. 1. Schematic Differences Between Apoptosis and Necroptosis

Licence- https://app.biorender.cm/illustrations/65cde4eb10cfa696f4157436

The apoptosis pathway involves the activation of caspases through intrinsic (mitochondrial) or extrinsic (death receptor) pathways, leading to cell dismantling. The necroptosis pathway highlights the role of receptor-interacting protein kinase 1 (RIPK1) and RIPK3 in mediating cell death independent of caspase activation. Upon apoptosis resistance (inactivation of caspase - 8), AIF is released from the mitochondria and transitions to the nucleus, causing mediated cell death parthanatos. Mediated pyroptosis is schematically illustrated and linked with necroptosis via RIPK3.

The critical importance of incorporating MRI tractography into preoperative planning for GBM surgery cannot be overstated. MRI tractography is a sophisticated imaging technique that visualizes the brain's white matter tracts, providing critical information about the neural pathways that may be at risk during tumor resection. In the case of the 63- and 65-year-old male patients diagnosed with malignant glioblastoma, MRI tractography was instrumental in mapping the proximity of the tumor to essential neural structures, enabling the neurosurgical team to plan a more precise and safer resection **(Fig. 2 A, B)** at MRC Hinduja Hospital, Mumbai, Neurosurgery Department.

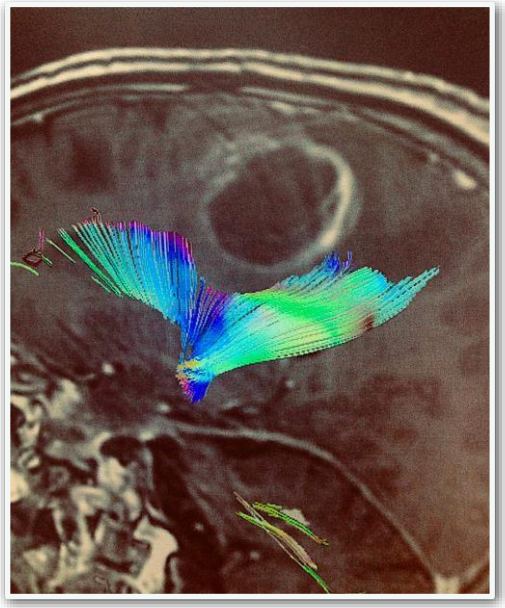

Fig. 2A. Patient's MRI - Tractography Scan

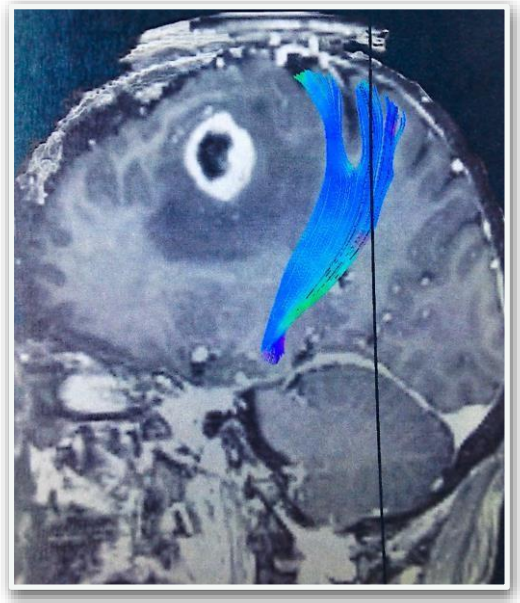

Fig. 2B. Patient's MRI - Tractography Scan.

The integration of MRI tractography in GBM surgery is particularly crucial due to the tumor's highly infiltrative nature. GBM often invades regions of the brain associated with vital functions, making it challenging to distinguish between tumor tissue and critical white matter tracts during surgery. By using MRI tractography, surgeons can identify and preserve these critical pathways, minimizing the risk of postoperative neurological deficits. This approach is essential for maintaining the patient's quality of life while striving for maximum tumor removal.

Moreover, when combined with PDT, MRI tractography enhances the precision of the surgical intervention. PDT with 5- ALA targets tumor cells specifically, leveraging their altered metabolic profile. The photosensitizer 5- ALA accumulates preferentially within glioblastoma cells, and when activated by intraoperative illumination, it generates ROS that selectively induce cytotoxic effects within the tumor. The precise mapping provided by MRI tractography ensures that PDT can be applied effectively while sparing the critical white matter tracts, which are essential for preserving neurological function.

This multimodal approach—combining MRI tractography with PDT—thus offers a comprehensive treatment strategy that not only enhances tumor control but also minimizes the risk of neurological deficits. The specificity of 5- ALA-mediated PDT, which targets glioblastoma cells while preserving surrounding healthy tissue, is well-aligned with the clinical goals of preserving cognitive and motor functions post-surgery.

Materials and Methods

Cell Culture

Glioblastoma (GBM) stem cell lines were maintained on Matrigel-coated plates in Advanced DMEM/F12 medium (Gibco) supplemented with 0.5% N2 supplement (Invitrogen), 1% B27 supplement (Invitrogen), 10 ng/mL fibroblast growth factor 2 (FGF2, Sigma), 4 µM heparin, 1% l-glutamine, and 20 ng/mL epidermal growth factor (EGF, Sigma). Cells were cultured in 75 cm^2 tissue culture flasks (Greiner Bio-One) at 37°C with 5 % CO_2 and harvested using Accutase (Sigma). All experiments utilized cells between passages 2 and 10, and cells were used when they reached 70-80% confluency, verified by microscopy (Leica Microsystems, Germany).

Photodynamic Therapy

Photodynamic therapy (PDT) was executed using a custom-built setup comprising an LEDD 1B-Cube LED Driver, DC2200-High-Power LED Driver, and mounted LEDs emitting at 415 nm (1310 mW) and 625 nm (700 mW) (Thorlabs, USA). Illumination was conducted within a light-tight metal enclosure to prevent exposure to stray light. Calibration of the optical setup was performed using a Thorlabs optical power meter (PM100D) and standardized conditions were maintained throughout the experiments. Additional photodynamic therapy (PDT) rigs (415 nm) were developed as a gift through a scientific collaboration involving Glasgow University, the University of Strathclyde, UK, and Dr. Akhill Kallepalli's lab team, including Graham Gibson and Royal Society Research Prof. Miles Padgett.

Viability Robotic Assay

GBM cells were seeded at 0.1×10^4 cells per well in Matrigel-coated 96-well plates (µClear, Greiner Bio-One) and incubated overnight. For PDT, 5-ALA, (Gliolan®, Medac) was prepared as a 30 mg/mL powder and added to a final concentration of 100 µM in Advanced DMEM/F12 medium. Cells were incubated with 5-ALA for 3 hours, then treated with SYTOX Green (1 µM, Invitrogen) immediately before illumination. PDT was performed using blue light at 415 nm with energy densities of 390 J/cm^2 (16 min, 4 s), 160 J/cm^2 (6 min, 3 s), and 100 J/cm^2 (4 min, 2 s). Post-illumination, cells were fixed with 4 % paraformaldehyde (PFA) at 20, 40, 60, and 80 min. Nuclei were counterstained with DAPI (1 µM, Sigma) and analyzed using the Opera Phenix® Plus High-Content Screening System (Perkin Elmer).

Clonogenic Assay

GBM stem cells were seeded at 30 (OX5) or 35 (G7) cells per well in Matrigel-coated 12 well plates. After overnight incubation, cells were treated with 5-ALA (100 μM) for 3 h, followed by PDT with energy densities of 390, 160, or 100 J/cm² as described. Post-PDT, plates were returned to the incubator for 10 days to allow colony formation. Colonies were fixed with methanol, stained with crystal violet, and manually counted using ImageJ software (Fiji, v2.1.4.0/1.54f).

Immunoblotting

Cells were lysed on ice in RIPA buffer (Thermo Fisher Scientific) supplemented with complete protease inhibitor cocktail and PhosSTOP (Roche). Protein concentration was quantified using the Pierce BCA Protein Assay Kit (Thermo Fisher Scientific). Lysates were resolved on 4-12 % NuPage Bis-Tris or SDS-PAGE gels (Thermo Fisher Scientific) and transferred onto nitrocellulose or PVDF membranes (pre-soaked in methanol) at 100V for 90 min or overnight at 25V. Membranes were blocked with 5% non-fat milk for 1 h and incubated overnight at 4°C with primary antibodies: Caspase-3 (#9662), Cleaved Caspase-3 (#9664), PARP1 (#9532), and β-actin (#8457) (Cell Signaling Technology), and p-MLKL (Ser 358) (#91689) and MLKL total (#14993) (Cell Signaling Technology), Anti-SOX2 antibody (#1791) Abcam 218520, GFAP (#3670S) (Cell Signaling Technology), α-Tubulin (#5335T) Rabbit mAb (Cell Signaling Technology), AIF Rabbit mAb (#5318), COX IV Rabbit mAb (#4850), PCNA (#13110) (Cell Signaling Technology). Membranes were washed in TBS-T and probed with HRP-linked secondary antibodies (anti-rabbit #7074, anti-mouse #7076; Cell Signaling Technology) for 1 h. Detection was performed using the Li-Cor Odyssey CLx system, and band intensities were quantified using Image Studio software (Li-Cor).

Mitochondrial Fractionation

Cells were seeded at 10 × 10⁶ cells, washed in cold PBS, and harvested using Accutase. Cell pellets were lysed with digitonin lysis buffer (1.25 mM sucrose, 3.3 mL PBS, 350 μL Tris Cl pH 8, 100 μg/mL digitonin) on ice for 20 min. Subsequent centrifugation at 3000g for 5 min at 4°C separated cytosolic and nuclear/mitochondrial fractions. The mitochondrial pellet was resuspended in RIPA buffer with protease and phosphatase inhibitors and incubated on ice for 20 min. After centrifugation at maximum speed for 20 min at 4°C, the supernatant containing the mitochondrial fraction was collected. Nuclear fractions were

obtained by resuspending the nuclear pellet in nuclear lysis buffer (50 mM Tris pH 8, 0.15 M NaCl, 1 % TritonX - 100, 0.02 % Na Azide) and processed as above.

Immunofluorescence Analysis

GBM stem cells were seeded at 10×10^3 cells/well on Matrigel-coated glass slides and incubated overnight. After treatment with 5-ALA (100 μM) for 3 h, cells were exposed to 415 nm PDT (390 J/cm²) and stained with MitoTracker Orange (500 nM, Invitrogen) for 30 min. Post-illumination, cells were fixed with 4 % PFA at 20, 40, 60 min, permeabilized with 0.01% Triton X-100, and incubated overnight at 4°C with anti-AIF primary antibody (1:400, Abcam). After washing, samples were incubated with Alexa Fluor 488-conjugated secondary antibody (1:500, Thermo Fisher Scientific) for 1 h in a dark hood. Nuclei were counterstained with DAPI and mounted using Fluoroshield (Abcam). Imaging was performed on a Zeiss LSM9 confocal microscope using Airyscan2 in Multiplex mode with Z-stack acquisition (9-10 sections per image). Colocalization analysis was conducted using ImageJ (Fiji).

Statistical Analysis

Statistical analyses were performed using Prism (v10.2.0, GraphPad Software). Data were analyzed by one-way or two-way ANOVA, followed by Tukey's post hoc test or Dunnett's test for multiple comparisons. Results were derived from at least three independent experiments, with significance set at $p < 0.05$.

Results

To rigorously evaluate the molecular selectivity of 5- ALA-mediated PDT in sparing healthy brain tissue, we hypothesized that 5-ALA-PDT would induce cell death exclusively in GSCs while leaving healthy astrocytes unaffected under clinically relevant conditions (160 J/cm²). To test this hypothesis, a comparative analysis using mouse astrocytes (mAS) and GSCs was conducted, aiming to replicate the clinical scenario by investigating whether 5-ALA- PDT triggers cytotoxic effects in non-tumor cells.

Western blot (WB) analysis was employed post-PDT to validate the molecular selectivity. The study specifically examined the expression of SOX2, a marker of stemness and malignancy, and GFAP, a marker of astrocytic differentiation. We postulated that SOX2 would be significantly downregulated in GSCs, indicating effective tumor cell targeting, while GFAP expression in mAS would remain stable, confirming the preservation of healthy astrocytes. This research provides a molecular framework to explore the safety and efficacy of 5-ALA-PDT in the clinical management of glioblastoma, offering insights into how this therapy can be optimized to improve patient outcomes.

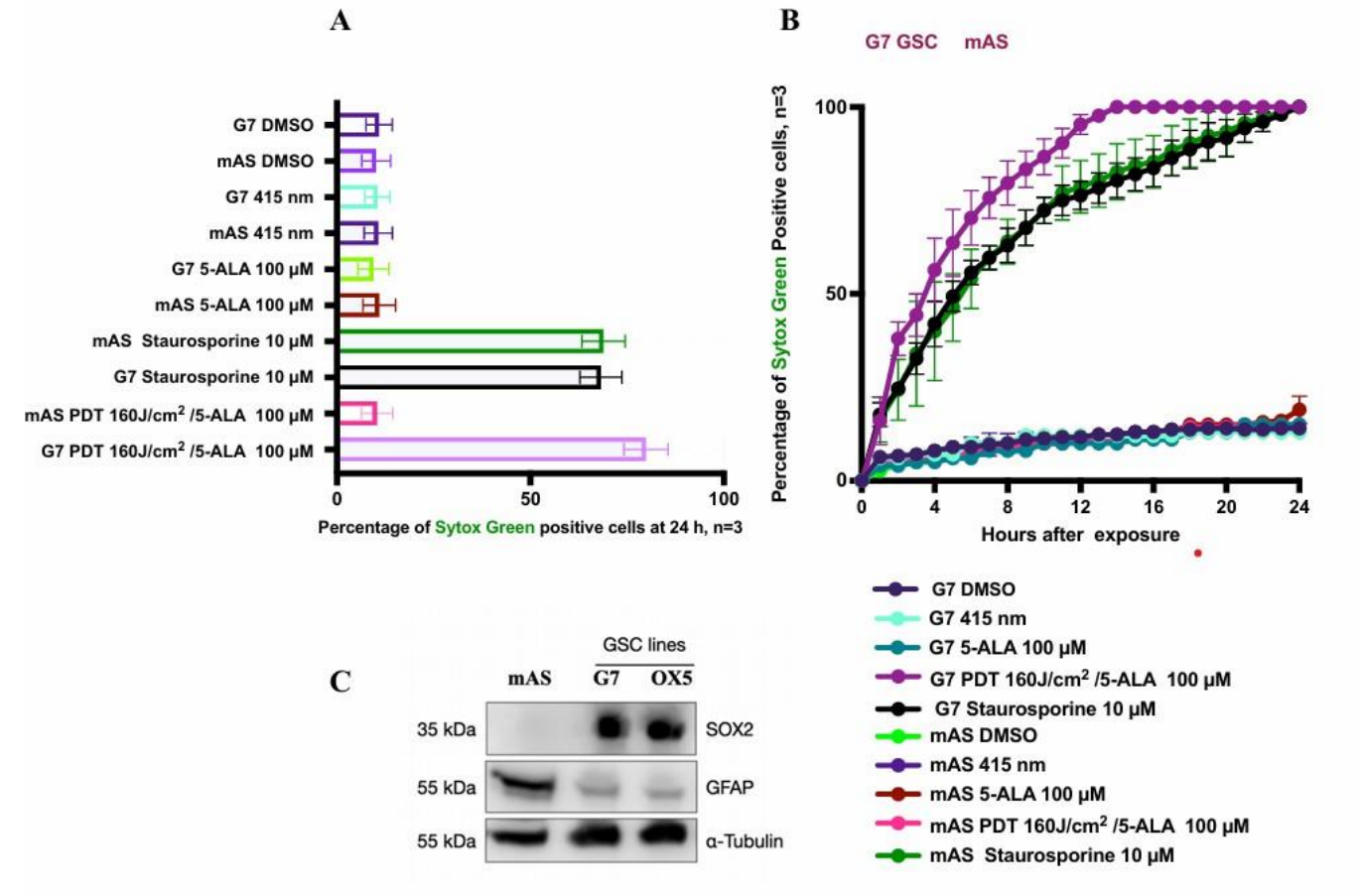

(A-B) IncuCute experiment: PDT/5-ALA treatment significantly reduces the viability of G7 glioma stem cells (G7), as evidenced by a marked decrease in cell survival compared to untreated controls ($p < 0.0001$, ANOVA). In contrast, mAS cells show no significant reduction in viability post-treatment, indicating that PDT does not adversely affect healthy brain tissue. Values normalised to Staurosporine 10 µM. Error bars represent the mean ± standard error of the mean (SEM). Statistical significance was determined using one-way ANOVA post hoc analysis.

(C) (WB) images showing SOX2 expression in G7, OX5 GSC and GFAP expression in mAS, results from three independent biological experiments (n = 3).

To address the inquiry regarding the cytotoxic effects of post-PDT/5- ALA treatment on GSCs, an Opera Phenix assay was conducted. This assay employed SYTOX Green fluorescence labelling to distinguish dying cells within the total cell count, marked with 4',6-diamidino-2-phenylindole (DAPI). Upon binding to the DNA of deceased cells, SYTOX Green elicited a discernible green fluorescence signal, thereby facilitating the identification and quantification of cell death events.

To investigate the cytotoxic effects specifically focused on cell death pathways, a fluence of 390 J/cm² was employed. Concurrently, clinical fluence rates of 100 J/cm² and 160 J/cm² were maintained to simulate therapeutic conditions. The concentration of 5-ALA used corresponded to a measured concentration of PpIX in resected brain tissue from a patient with glioblastoma, which was approximately 100 µM (Sharayu Chandratre et al, 2024).

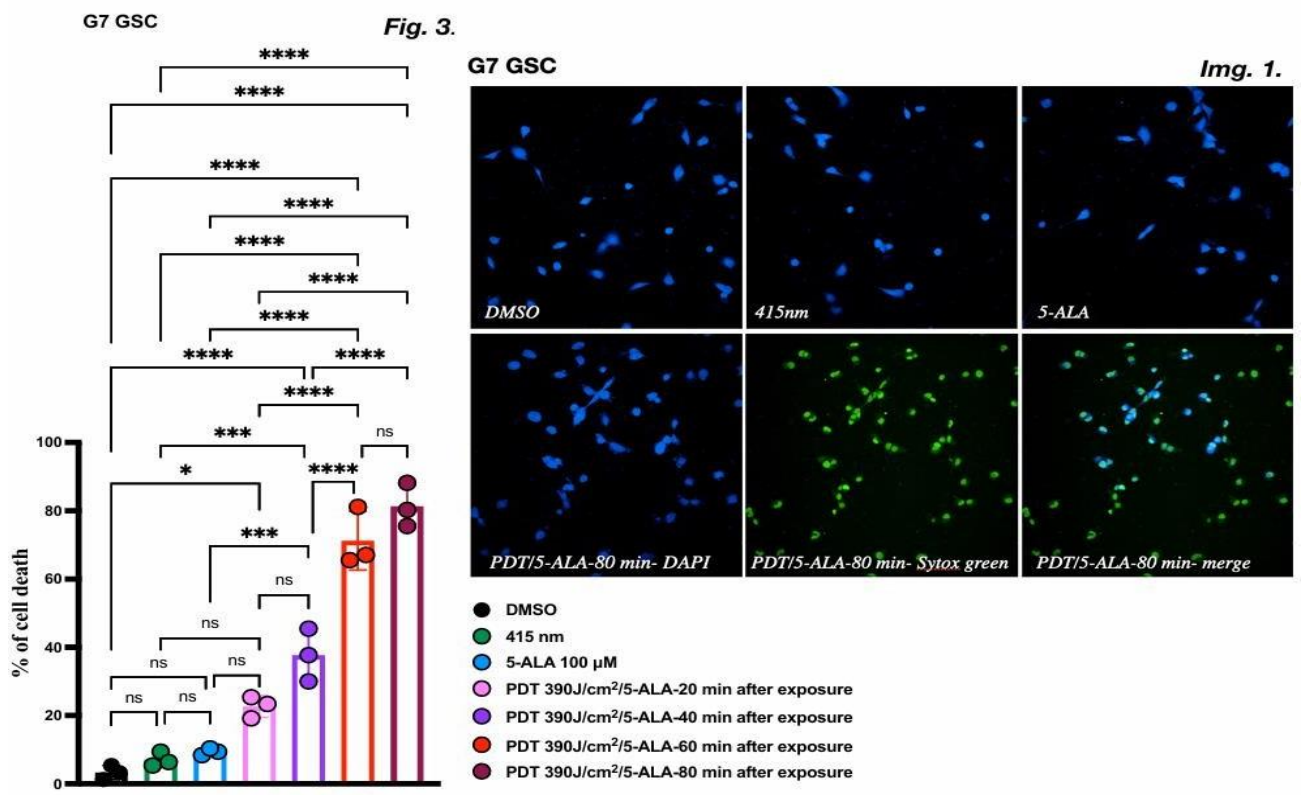

Cytotoxic effect of PDT/5- ALA in G7 GSC in time-dependent manner **(Fig. 3).** Values represent 3 biologically independent experiments in G7 GSC. The percentage of cell death was calculated using Opera Phenix, SYTOX Green (cell death marker), and DAPI (total cell count)- **(Img.1).** 0ne-way Anova analysis, if alpha > 0.05, indicated statistical significance between DMSO, 415 nm, 5- ALA vs. PDT 390 J/cm2/5-ALA (**** p<0.0001), followed by Tukey's post-hoc analysis (**** p<0.0001). NS (p>0.9999, p>0.9837). Error bars represent +/-SD from 3 independent experiments.

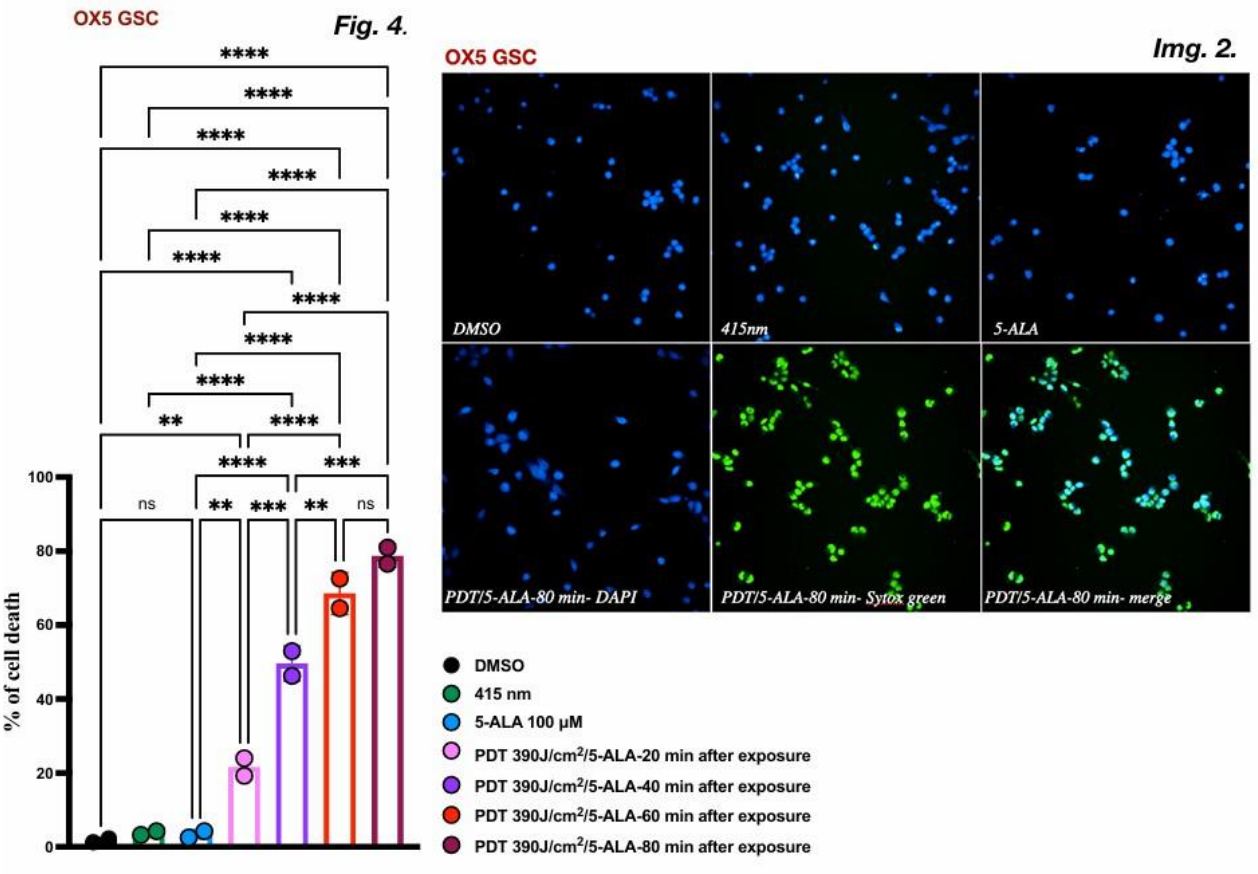

Potent cytotoxic effect of PDT/5- ALA in OX5 GSC in time-dependent manner. Values represent 2 biologically independent experiments in OX5 GSC **(Fig.4).** The percentage of cell death was calculated by Opera Phenix using SYTOX Green (cell death marker) and DAPI (representing total cell count)- **Img.2**. A one-way ANOVA analysis was performed, and if alpha was greater than 0. 05, statistical significance between DMSO, 415 nm, 5-ALA vs. PDT 390 J/cm2/5-ALA was determined (**** p>0.9946, p>0.9981). Error bars represent +/- SD from 2 independent experiments.

Similarly, OX5 GSC demonstrated significant cell death at 80 minutes post-PDT/5-ALA **(Fig. 4)**. **Img. 2** - representative image after exposure in OX5 GSC from Opera Phenix analysis.

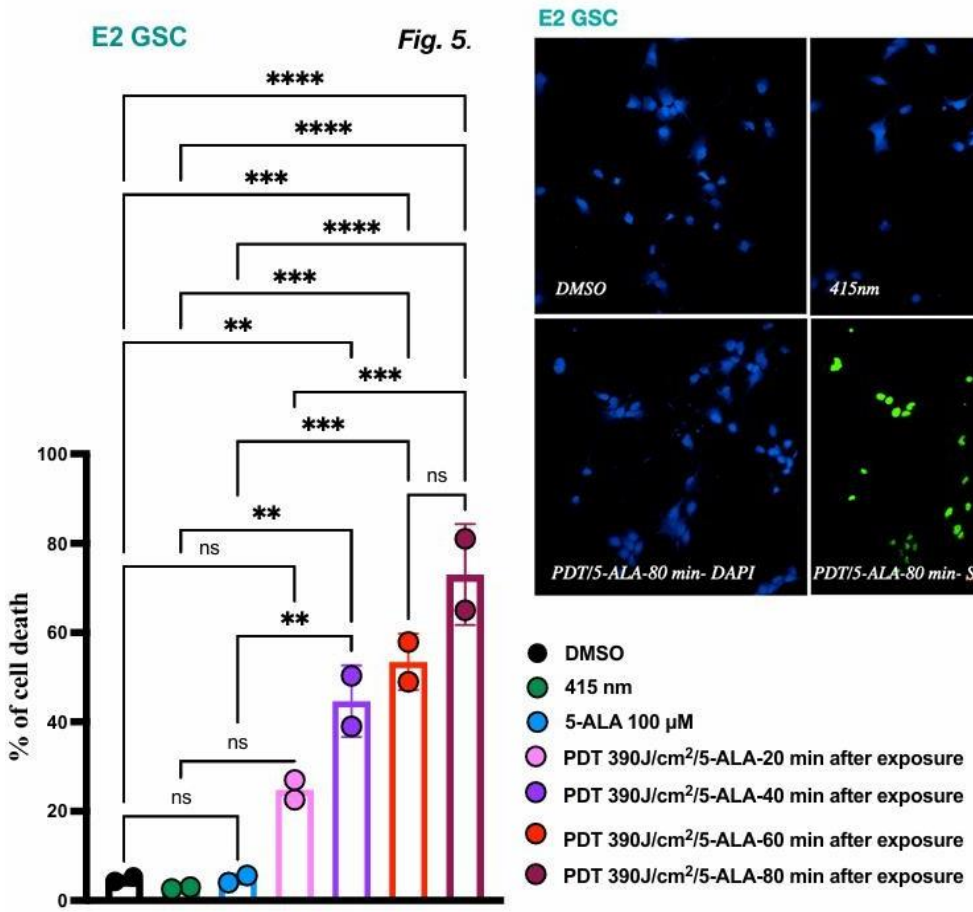

Cytotoxicity of PDT/5-ALA is presented in E2 GSC in a manner dependent on time **(Fig. 5).** Values represent 2 biologically independent experiments in E2 GSC. Percentage of the cell death was calculated by Opera Phenix using SYTOX Green (cell death marker) and DAPI (represents total cell count) - **Img.3**. 0ne-way Anova analysis, if alpha > 0.05, statistical significance between DMSO, 415 nm, 5- ALA vs. PDT 390 J/cm2/5-ALA (**** p>0.9946, p>0.9999, p>0.0983). Error bars represent +/-SD from 2 independent experiment.

E2 GSC demonstrated significant cell death at 80 minutes post-PDT/5-ALA **(Fig.5). Img.3** -representative image after exposure in E2 GSC from Opera Phenix robotic analysis.

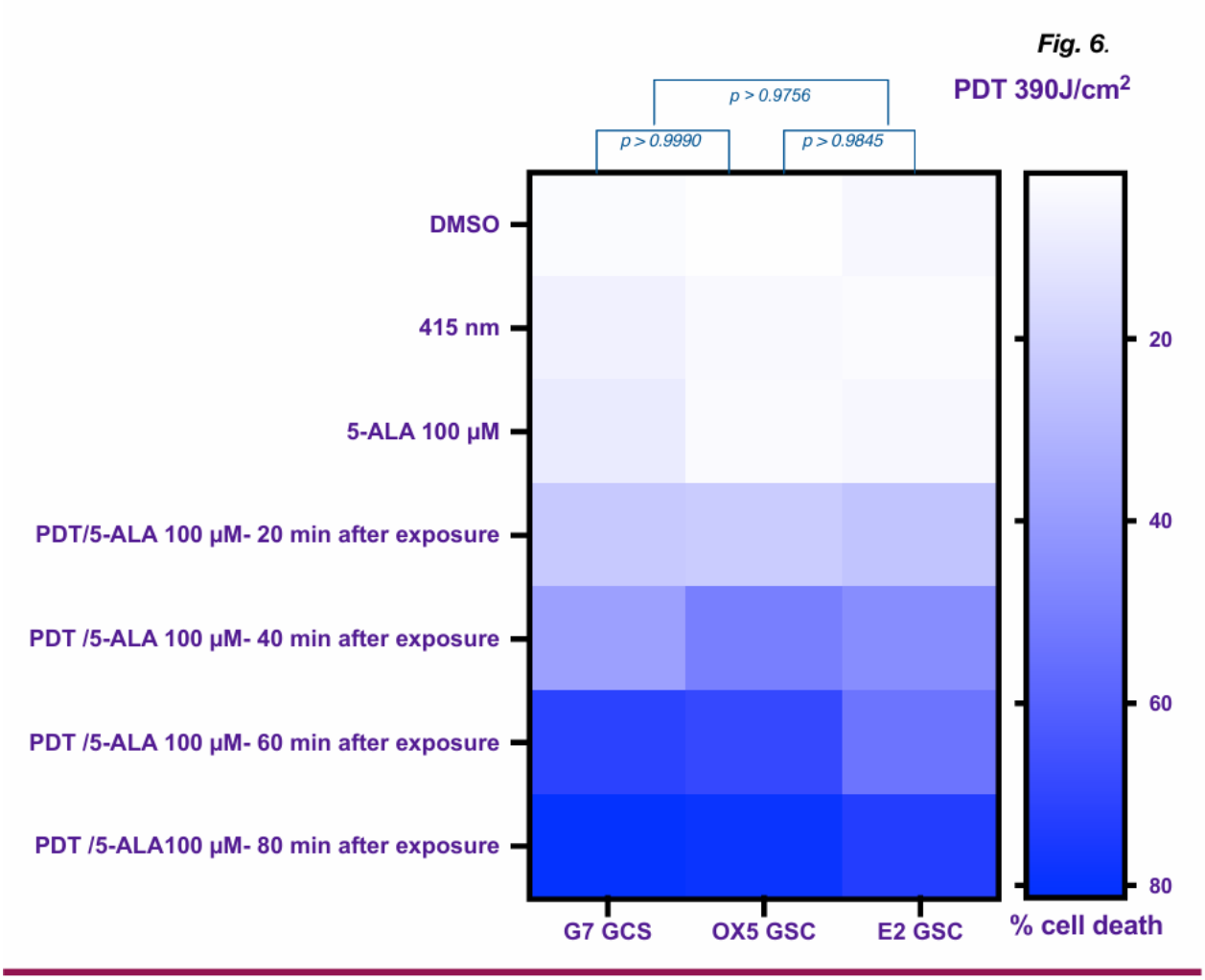

The heatmap represents the mean of three patient-derived GSC lines **(Fig.6)**. The time (20, 40, 60, 80 min) after the fluence rate (J/cm2) demonstrates the percentage of cell death after exposure to PDT. Cells were treated with +/-PDT/5-ALA and analysed by robot (Opera Phenix) using SYTOX Green and DAPI. Analysis performed using one-way Anova, followed by Tukey's test indicating no statistical significance before treatment between GSC lines (NS, p> 0.9990, p>0.9756, p> 0.9845) and after PDT/5-ALA-80 min (length of time after exposure to PDT) between G7 vs. OX5, G7 vs. E2, OX5 vs. E2 GSCs (NS, p>0.2426, p>0.4001, p>0.2701). The two-way ANOVA analysis conducted on G7, OX5, and E2 GSCs revealed significant cell death across the specified time points, with a notable difference observed between treatment groups: DMSO, 415nm, and 5-ALA versus 390 J/cm2 415 nm PDT/5-ALA (****p<0.1394). N=3 independent experiments in G7 GSC, N=2 independent experiments in OX5 and E2 GSCs.

While GSCs are a subpopulation of cancer cells within gliomas that possess stem cell-like properties, such as self-renewal and differentiation capacity, and the clonogenic assay assesses the ability of single cells to form colonies, providing a measure of long-term cell survival, I conducted experiments to determine whether GSCs can lose their stemness after exposure to PDT/5- ALA at different fluence rates (J/cm2) over a period of 10 days following illumination.

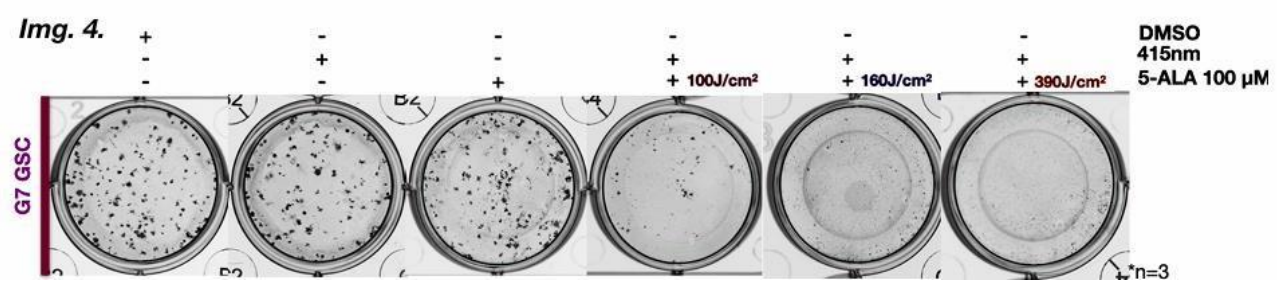

G7 GSC

Fig. 7.

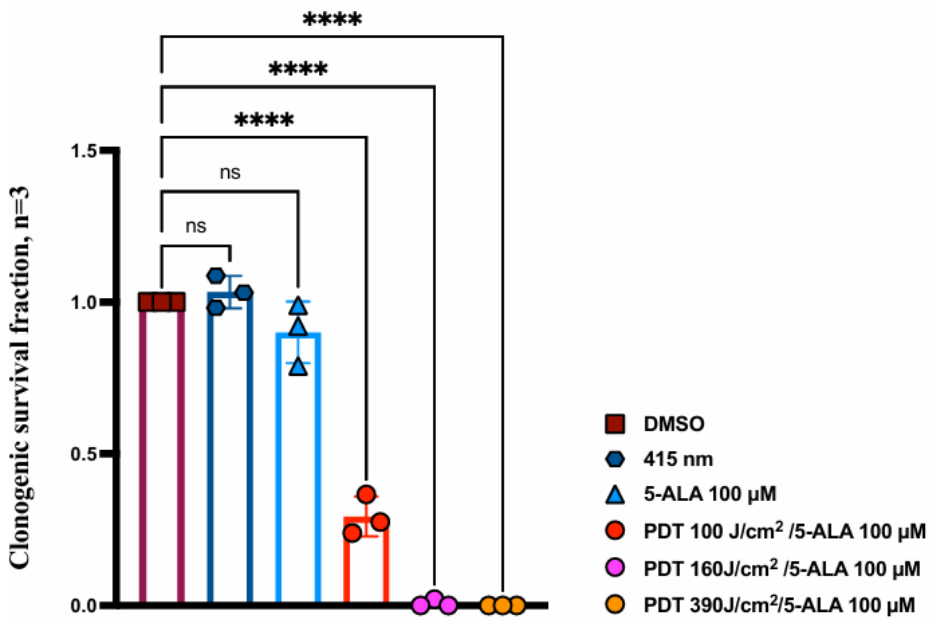

Clonogenic analysis shows G7 GSC treated +/-PDT/5-ALA **(Fig. 7).** Images from 3 independent experiments scanned using the LICOR imager. The colonies formed over an experimental period of 10 days. Values analysed using 0ne-way Anova analysis, if alpha > 0.05, statistical significance between DMSO, 415 nm, 5- ALA vs. PDT 100/160/390 J/cm2/5 ALA , (**** p>0.9850, p>0.9999). Error bars represent +/- SD. 390 J/cm2 and 160 J/cm2 demonstrated potent cytotoxic effect after PDT/5-ALA with no colonies **(Fig.7).**

Img. 4 -Representative scanned image of G7 GSC.

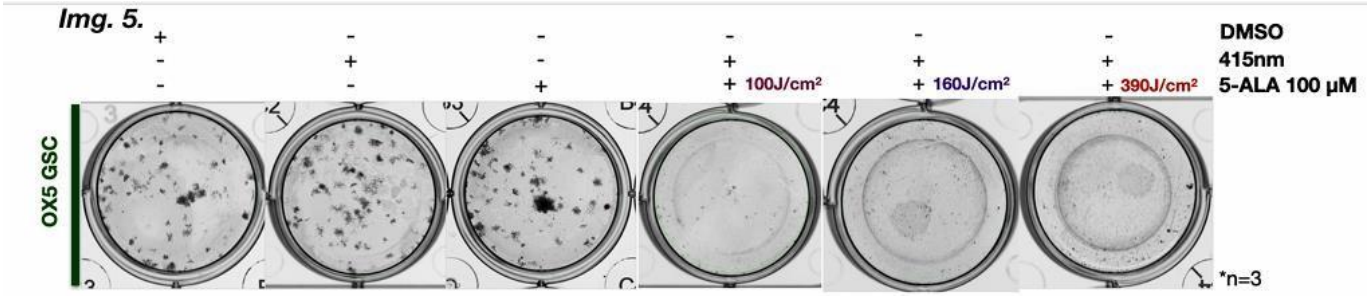

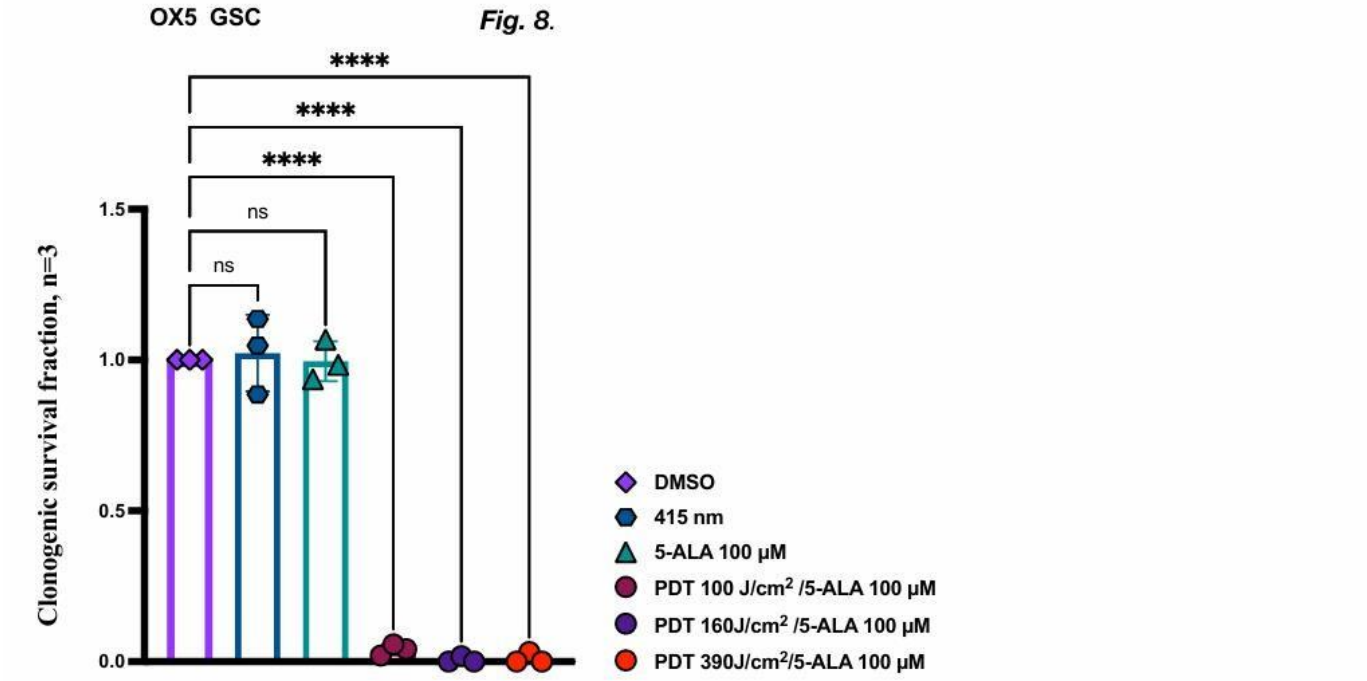

Clonogenic analysis demonstrates OX5 GSC treated +/-PDT/5-ALA **(Fig. 8).** Images from 3 independent experiments scanned using the LICOR imager. The colonies formed over an experimental period of 10 days. Values analysed using 0ne-way Anova analysis, if alpha >0.05, statistical significance between DMSO, 415 nm, 5- ALA vs. PDT 100/160/390 J/ cm2/5-ALA, (**** p>0.9075, p> 0.1510). Error bars represent +/- SD.

390/160/100 J/cm2 PDT/5-ALA demonstrated cytotoxic effect with no colonies in OX5 GSC **(Fig. 8).**

Img. 5 -Representative scanned image of OX5 GSC.

Next, to delve deep into the cell death mechanism, experiments with cell death inhibitors were employed, such as the necroptosis inhibitor Necrosulfinamide (NSA) and the caspase- 3 inhibitor (Z-DEVD-FMK). These inhibitors can assist in elucidating the specific cell death pathways involved in the response to PDT/5-ALA treatment.

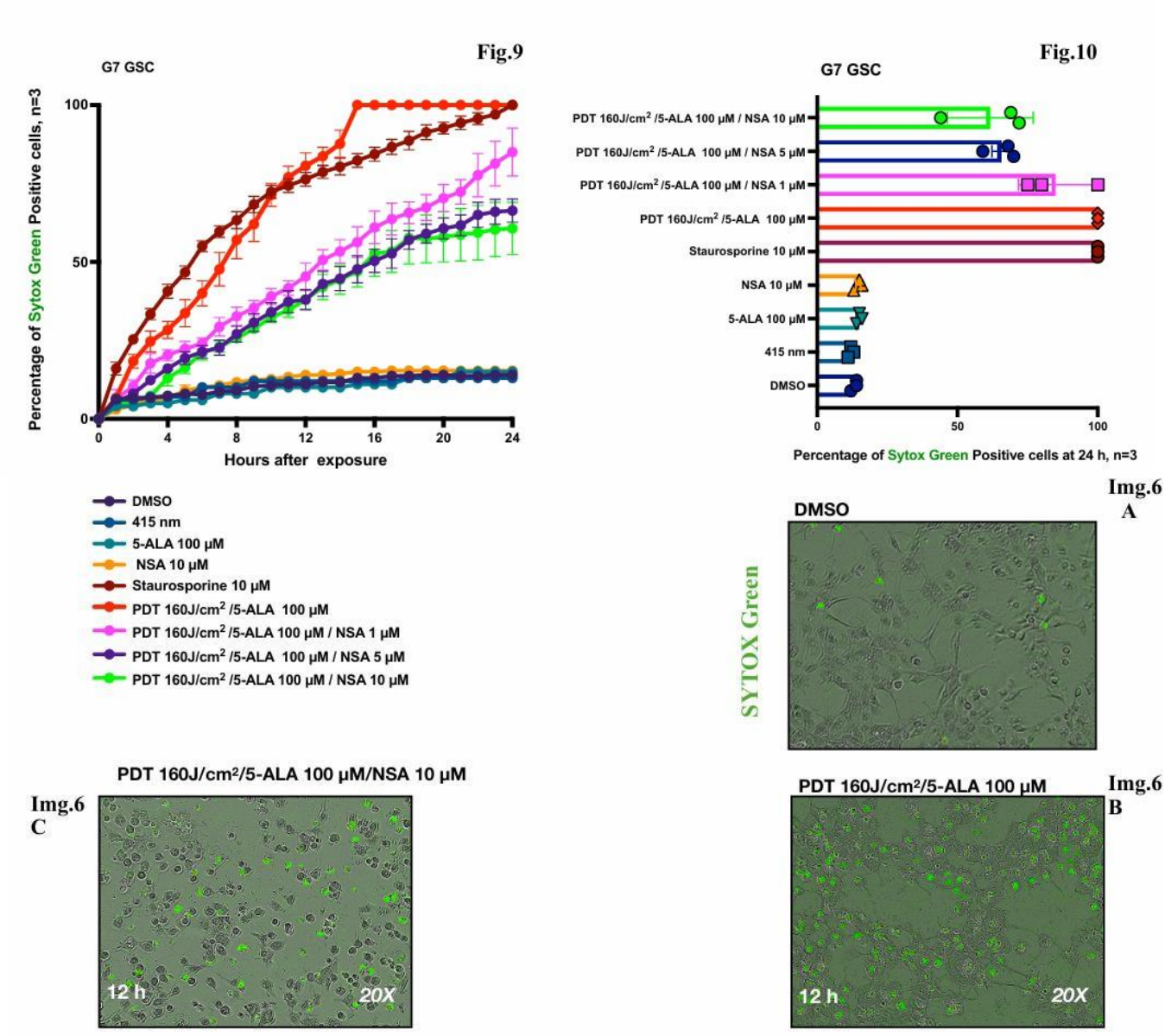

The Incucyte experiment depicted in **(Fig. 9, 10)** illustrates the response of G7 GSCs to PDT/5- ALA treatment with/ without NSA. Values represent 3 biologically independent experiments, % of SYTOX Green Positive cells were calculated from total cell count - values normalised with G7 GSC treated with 10 µM Staurosporine. Error bars represent +/-SEM. Two-way Anova analysis, if alpha > 0.05, statistical significance between DMSO, 415 nm, 5-ALA vs. PDT 160J/cm2/5-ALA, (****p>0.9999) between DMSO,

415nm, 5-ALA, NSA 10 µM **(Fig. 9, Fig. 10). Img. 6A**- representative G7 GSC treated with DMSO -12 h after exposure to PDT. **Img. 6B**- representative G7 GSC treated with 5-ALA and exposed to PDT- 12 h after exposure. **Img. 6C**- representative G7 GSC treated with 5-ALA (3 h incubation time) and NSA 10 µM - 40 min prior exposure to PDT.

Inhibiting G7 GSCs with NSA at indicated concentrations after PDT treatment suggests a potential involvement of necroptosis pathway in the cell death mechanism elicited by the treatment regimen **(Fig. 9, Fig. 10).**

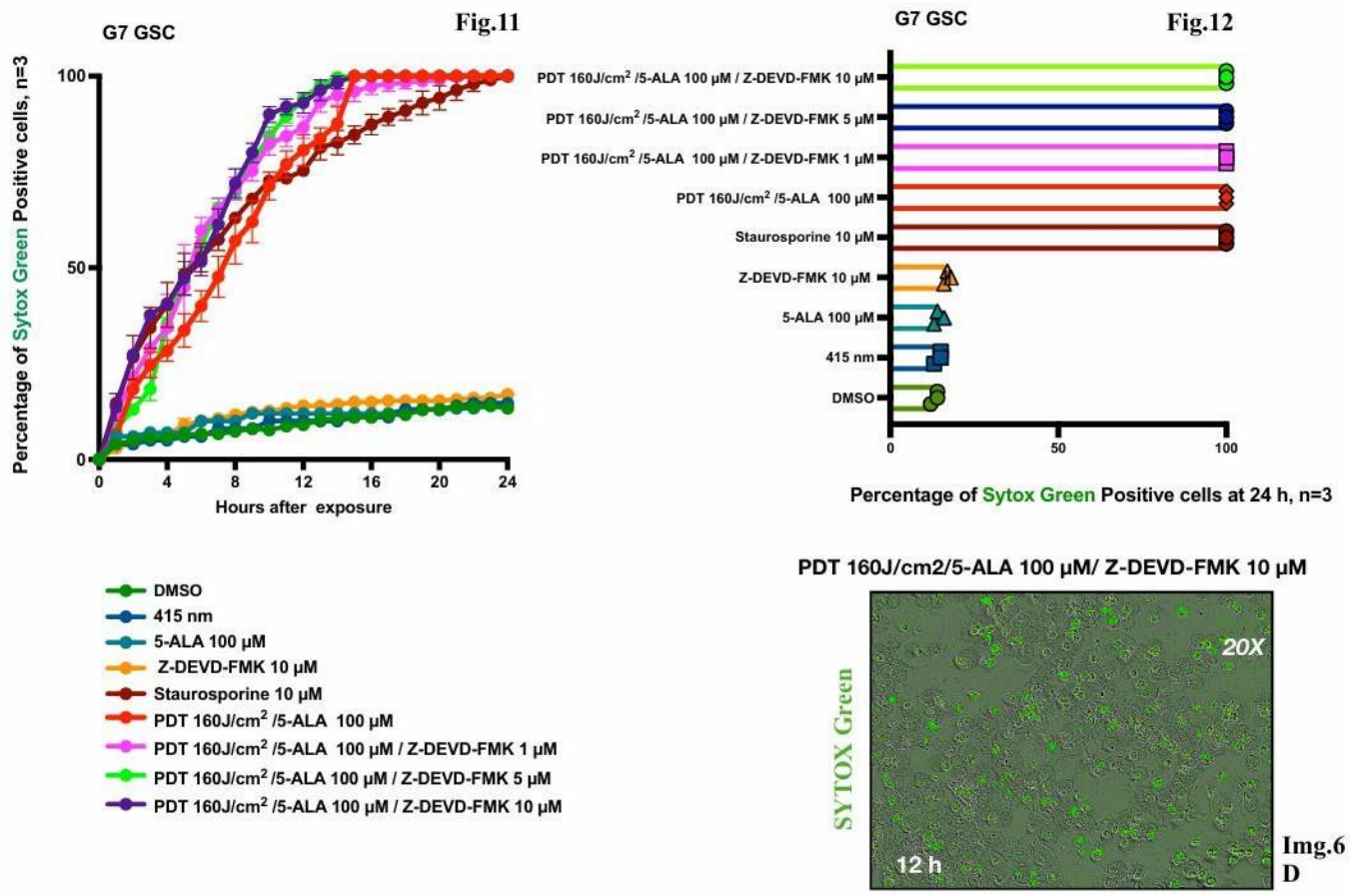

The Incucyte experiment depicted in **(Fig. 11, 12)** showcases the response of G7 GSCs to PDT/5-ALA treatment with/ without Z-DEVD-FMK. Values represent 3 biologically independent experiments, % of SYTOX Green Positive cells were calculated from total cell count -values normalised with G7 GSC treated with 10 µM Staurosporine. Error bars represent +/-SEM. Two-way Anova analysis, if alpha > 0.05, statistical significance between DMSO, 415nm, 5- ALA vs. PDT 160J/cm2/5- ALA, (****p>0.9999,p>0.9998, p>0.9988)- **(Fig. 11, Fig. 12).** No significance between PDT

160 J/cm2/5- ALA vs. PDT 160 J/cm2/5- ALA/Z- DEVD- FMK at indicated concentrations (ns, p>0.2502, p>0.4916, p>0.4109). **Img.6D**- representative G7 GSC treated with 5- ALA (3 h incubation time) and Z DEVD-FMK 10 µM - 40 minprior exposure to PDT.

The ineffectiveness of Z-DEVD-FMK in inhibiting G7 GSCs post-PDT, coupled with the immediate cell demise, suggests a non-apoptotic mode of cell death predominance **(Fig.11, 12).** This outcome underscores the likelihood of alternative cell death pathway(s), potentially implicating necroptosis and other mediated mechanisms, thereby illustrating the intricate cellular response to PDT treatment in G7 GSC.

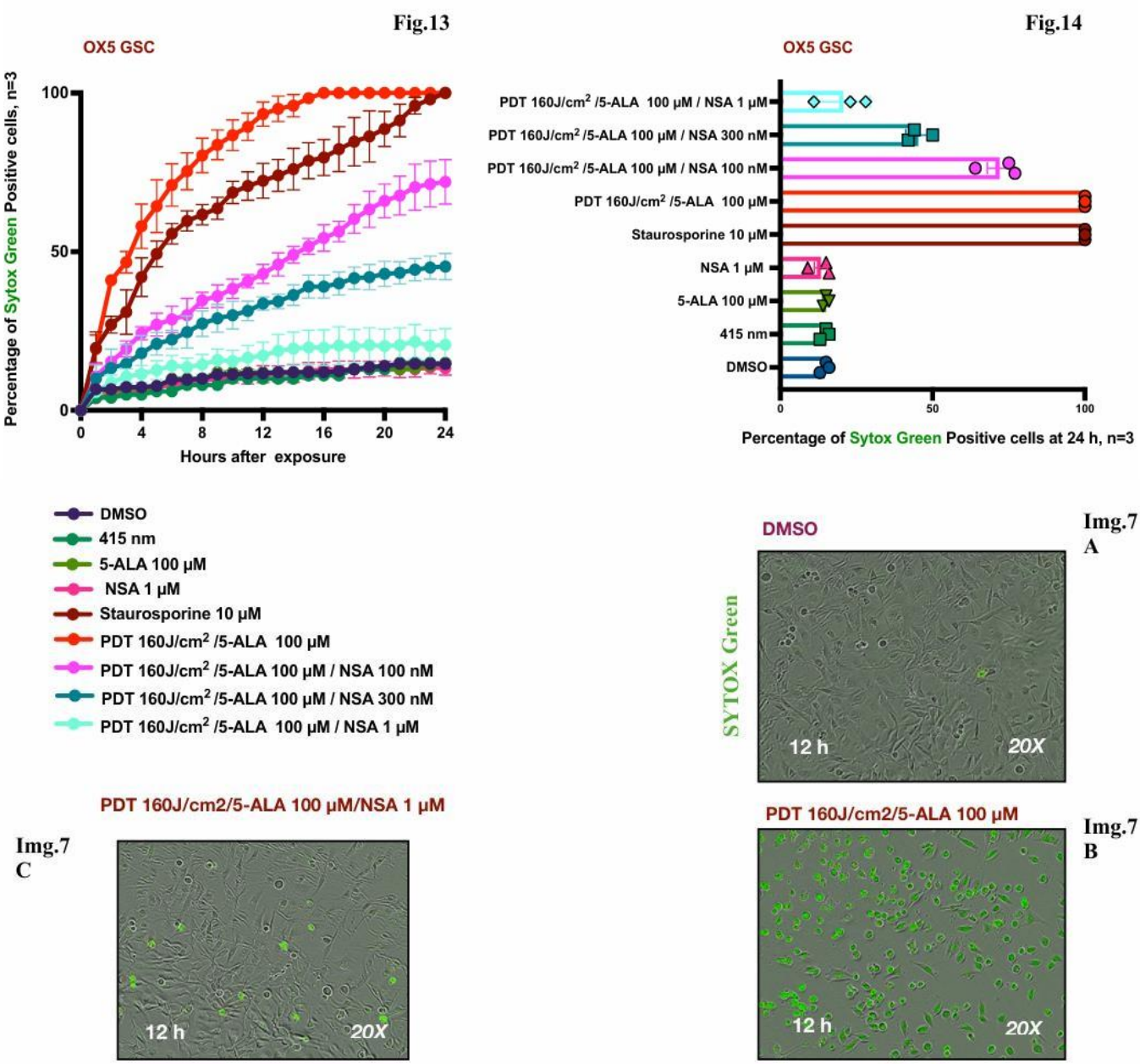

As observed in the Incucyte experiment **(Fig. 13 and 14)** illustrate the response of OX5 GSCs to PDT/5-ALA treatment, with or without the addition of NSA. Values represent 3 biologically independent experiments, % of SYTOX Green Positive cells were calculated from total cell count -values normalised with OX5 GSC treated with 10 µM Staurosporine. Error bars represent +/-SEM. Two-way Anova analysis, if alpha>0.05, statistical significance between DMSO, 415 nm, 5-ALA vs. PDT 160J/cm2/5-ALA, (****p>0.9999) between DMSO, 415 nm, 5-ALA, NSA 1 µM. **(Fig. 13, Fig. 14). Img. 7A**-representativeOX5 GSC treated with DMSO -12 h after exposure to PDT. **Img. 7B-** representative OX5 GSC treated with5-ALA and exposed to PDT- 12 h after exposure**. Img. 7C-** representative OX5 GSC treated with 5-ALA (3 h incubation time) and NSA 1 µM - 40 min prior exposure to PDT.

Inhibiting OX5 GSCs with NSA at indicated concentrations after PDT treatment demonstrates involvement of necroptosis pathway in the cell death mechanism post-PDT/5-ALA treatment regimen **(Fig. 13, Fig. 14)**.

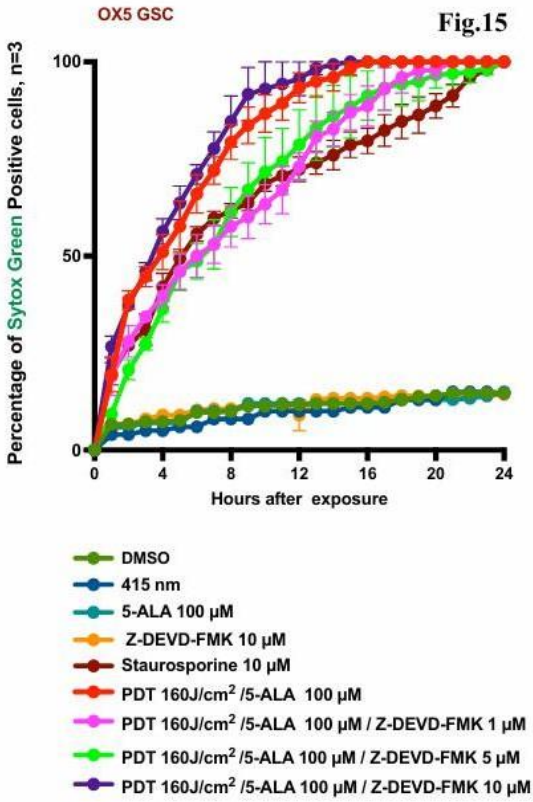

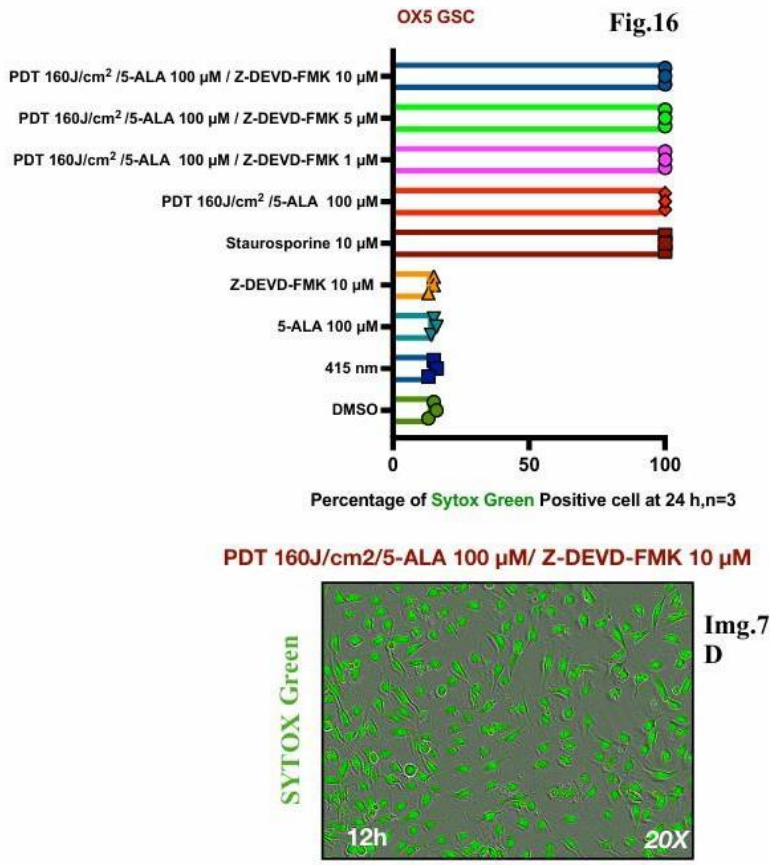

The experiment conducted in the Incucyte, as shown in **Fig. (15, 16),** demonstrates how OX5 GSCs respond to +/-PDT/ 5-ALA treatment, both with and without the presence of Z-DEVD-FMK. Values represent 3 biologically independent experiments, % of SYTOX Green Positive cells were calculated from total cell count -values normalised with OX5 GSC treated with 10 µM Staurosporine. Error bars represent +/-SEM. Two-way Anova analysis, if alpha > 0.05, statistical significance between DMSO, 415 nm, 5- ALA vs. PDT 160 J/cm2/5 ALA, (****p>0.9999, p>0.9998, p>0.9988) - **(Fig. 15, Fig. 16).** No significance between PDT 160 J/cm2/5-ALA vs. PDT 160 J/cm2/5- ALA/Z-DEVD-FMK 10 µM (ns, p>0.2502). **Img. 7D**-representative OX5 GSC treated with 5-ALA (3 h incubation time) and Z- DEVD- FMK 10 µM - 40 min prior exposure to PDT.

The failure of Z-DEVD-FMK to inhibit caspase- 3 in OX5 GSCs following PDT, alongside immediate cell death, indicates a non-apoptotic mode of cell death predominance **(Fig. 15, 16).** This suggests the involvement of alternative cell death pathways, potentially implicating necroptosis and other mediated mechanisms, illustrating the complex cellular response to PDT treatment in OX5 GSC.

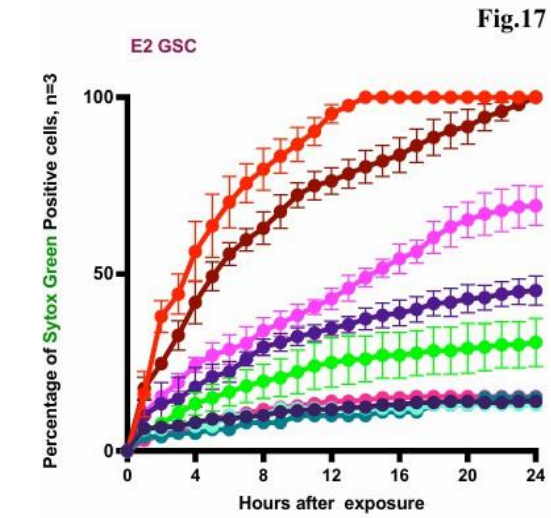

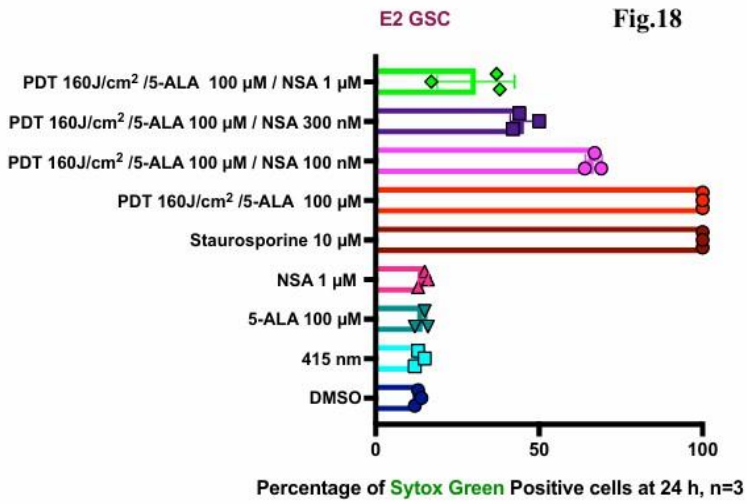

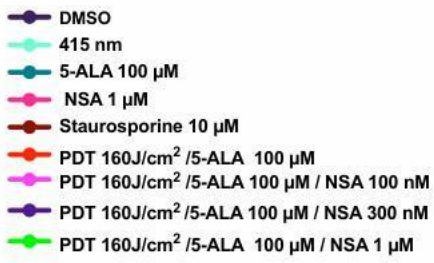

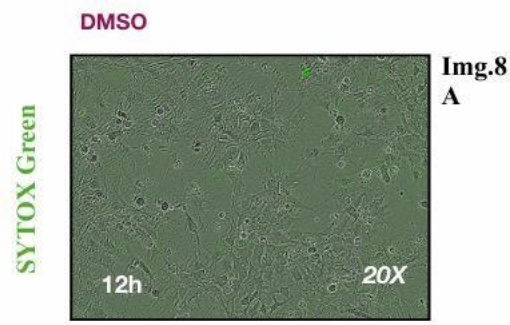

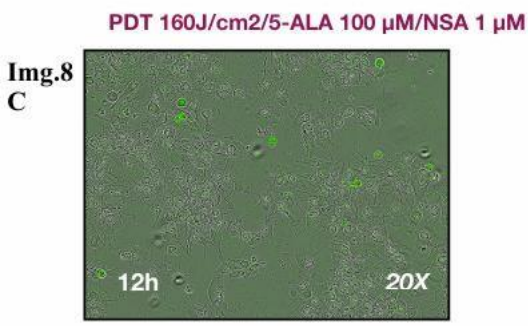

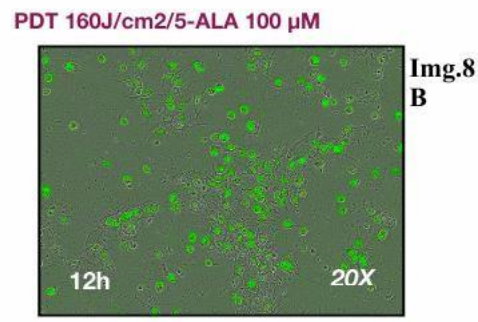

The response of E2 GSCs to +/-PDT/5-ALA treatment, with or without the inclusion of NSA, is illustrated in the Incucyte experiment depicted in **(Fig. 17, 18).** Values represent 3 biologically independent experiments, % of SYTOX Green Positive cells were calculated from total cell count -values normalised with E2 GSC treated with 10 µM Staurosporine. Error bars represent +/-SEM. Two-way Anova analysis, if alpha >0.05, statistical significance between DMSO, 415nm, 5-ALA vs. PDT 160J/cm2/5-ALA, (****p>0.9999) between DMSO, 415nm, 5-ALA, NSA 1 µM. **(Fig. 17, Fig. 18). Img. 8A**-representative E2 GSC treated with DMSO -12 h after exposure to PDT. **Img. 7B**- representative E2 GSC treated with 5-ALA and exposed to PDT- 12 h after exposure. **Img. 7C**- representative E2 GSC treated with 5-ALA (3 h

incubation time) and NSA 1 µM - 40 min prior exposure to PDT.

The inhibition of E2 GSCs post-PDT/5-ALA treatment may potentially activate the necroptosis pathway **(Fig. 17, 18).**

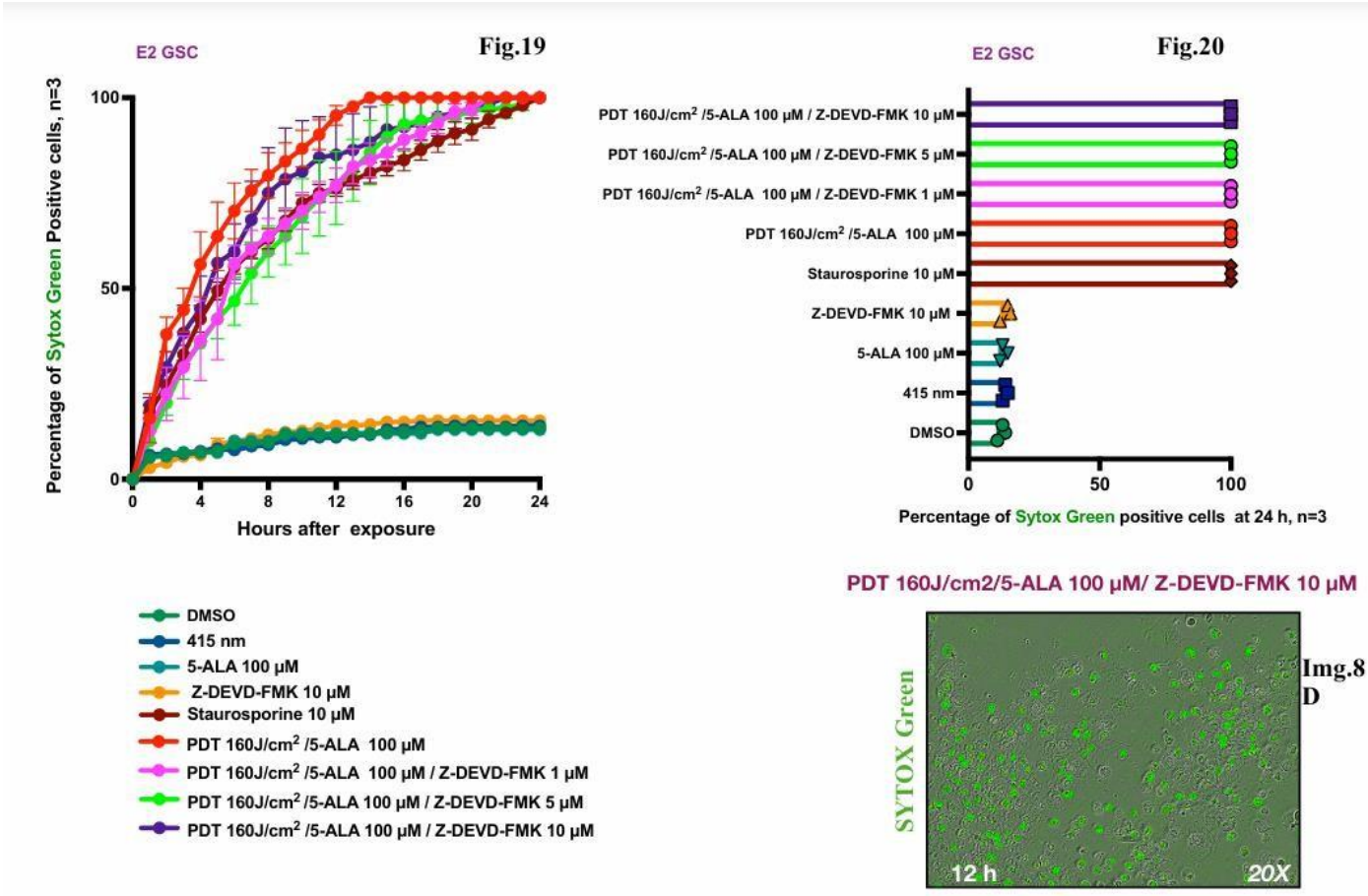

In the Incucyte experiment, (Fig. 19 and 20) present the observed reaction of E2 GSCs to +/-PDT/5-ALA treatment, both with/without the addition of Z-DEVD-FMK. Values represent 3 biologically independent experiments, % of SYTOX Green Positive cells were calculated from total cell count -values normalised with E2 GSC treated with 10 µM Staurosporine. Error bars represent +/-SEM. Two-way Anova analysis, if alpha > 0.05, statistical significance between DMSO, 415nm, 5- ALA vs. PDT 160 J/cm2/5-ALA, (***p>0.9999, p>0.9987, p>0.9985) **-(Fig. 19, 20).** No significance between PDT 160 J/cm2/5-ALA vs. PDT 160J/cm2/5-ALA/Z-DEVD-FMK 10 µM (ns, p>0.4916)- **(Fig. 19, 20). Img. 8D**- representative E2 GSC treated with 5-ALA (3 h incubation time) and Z-DEVD-FMK 10 µM - 40 min prior exposure to PDT.

Z-DEVD-FMK was ineffective in inhibiting caspase-3 in E2 GSC following PDT/5-ALA treatment,

indicating that the apoptosis pathway was not activated in this cell line after exposure to PDT- **(Fig. 19, 20).**

To further investigate the potential involvement of the necroptosis pathway in GSCs post-PDT/5 ALA treatment, Western blot analysis was conducted. This analysis aimed to assess the protein expression levels and activation status of key components implicated in cell death events, as well as to elucidate the main differences between necroptosis and apoptosis pathways.

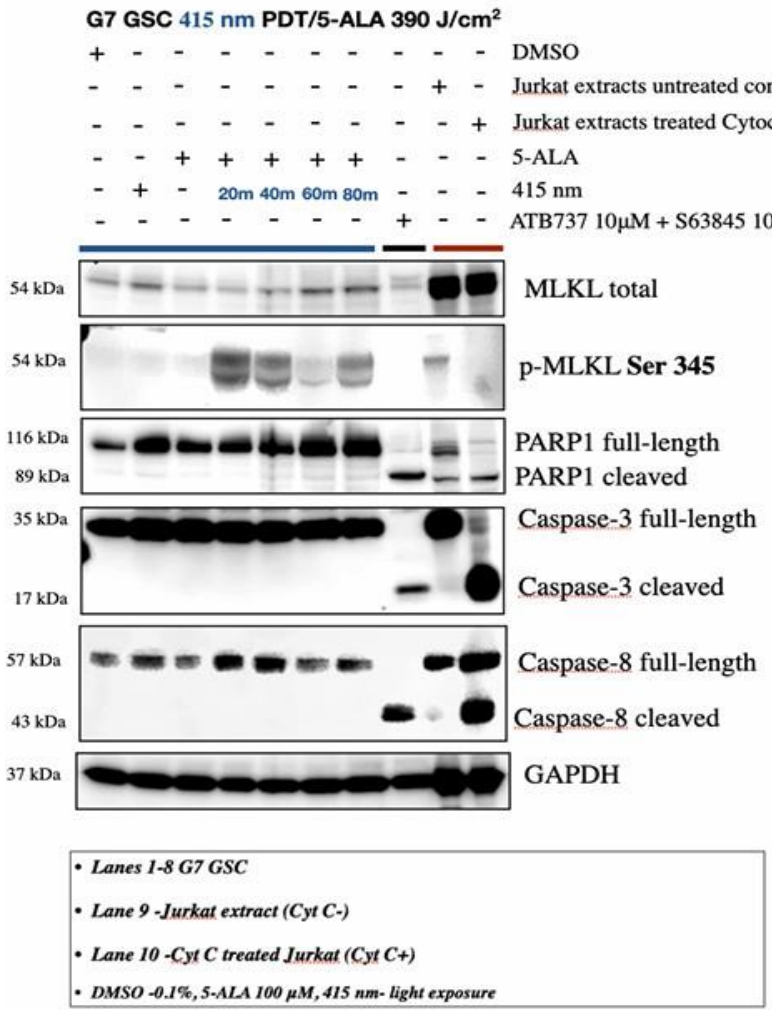

Fig.21

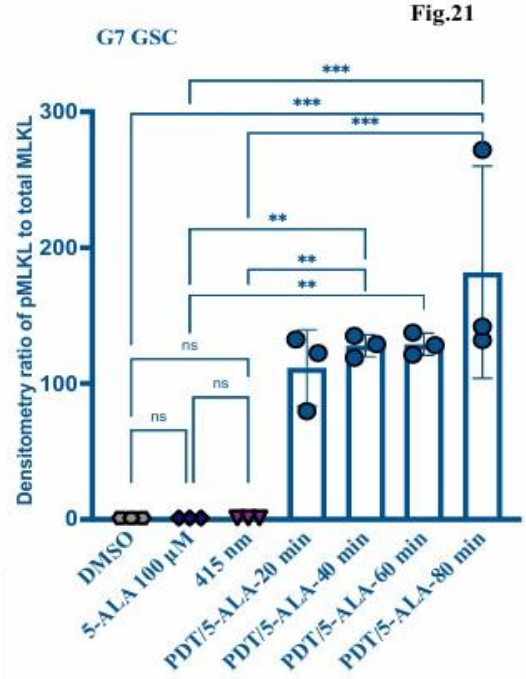

G7 GSC PDT 415nm /5-ALA-80 min **img9.**

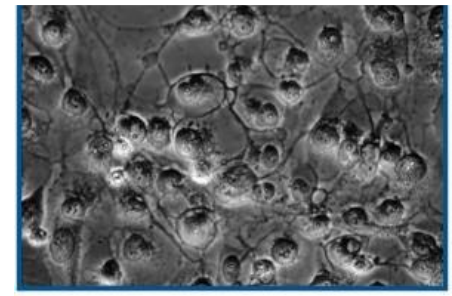

WB images represent Necroptosis pathway activation in G7 GSC. Data from 3 biologically independent experiments. One-way Anova analysis represents significance in G7 GSC treated with DMSO, 415nm, 5-ALA vs. PDT 390 J/ cm_2/5-ALA at indicated time points (***p < 0.0001), followed by Tukey's post hoc analysis (***P < 0.0001), error bars represent +/-SD in 3 independent experiments - **(Fig. 21). Img. 9-** Representative image of G7 GSC 80 min post PDT/5-ALA taken using Zeiss Microscope (Leica Microsystem, Germany) at 40x.

TUKEY'S HSD	Adjusted P Value
DMSO vs. 5-ALA 100 µM	>0.9999
DMSO vs. 415 nm	>0.9999
DMSO vs. PDT/5-ALA-20 min	0.0105
DMSO vs. PDT/5-ALA-40 min	0.0034
DMSO vs. PDT/5-ALA-60 min	0.0031
DMSO vs. PDT/5-ALA-80 min	0.0001

- The presence of p-MLKL at Serine 345 suggests activation of the necroptosis pathway following PDT/5-ALA treatment, thereby excluding the involvement of apoptotic death events in G7 GSC post-exposure.

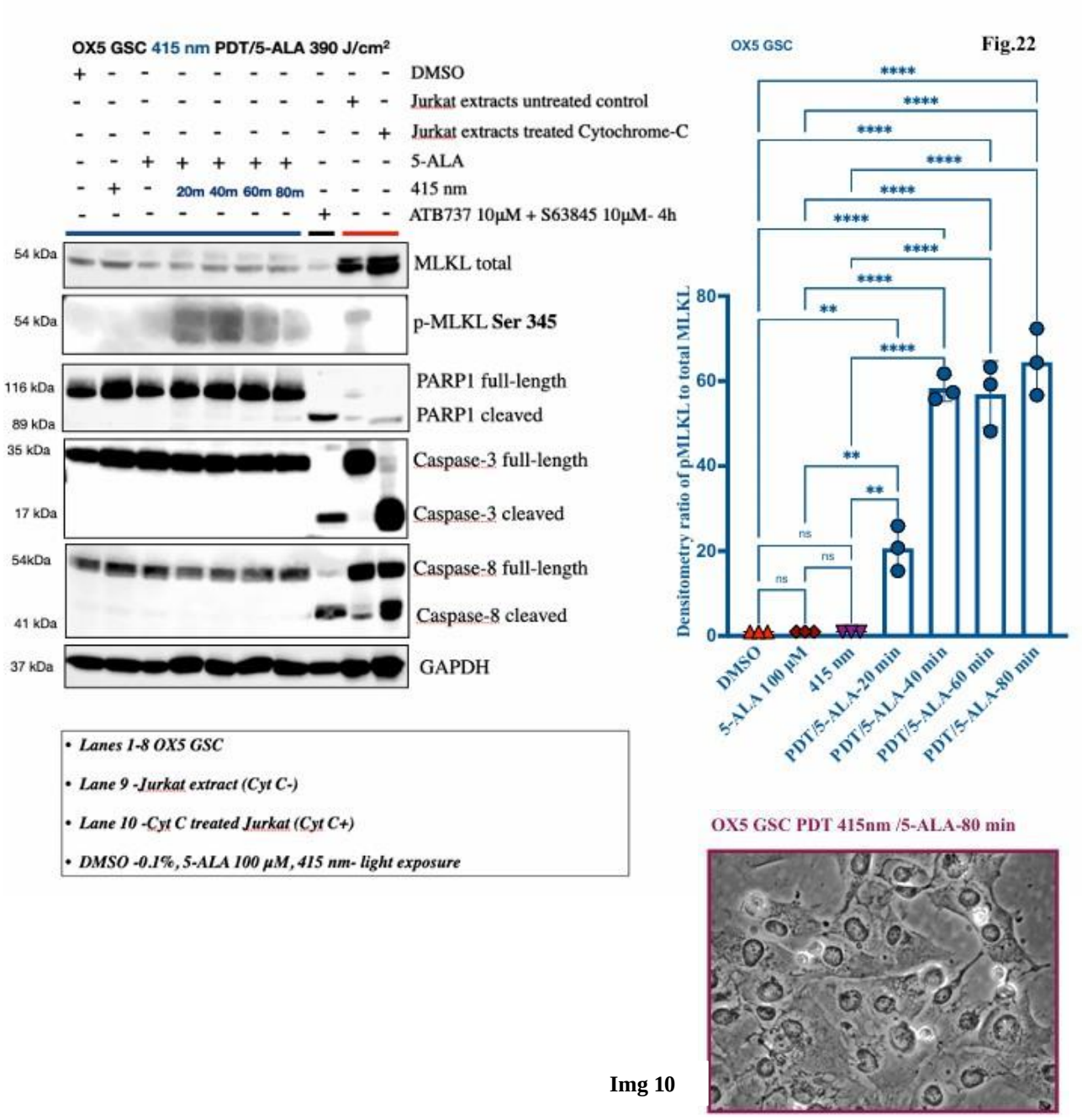

Img 10

WB images represent Necroptosis pathway activation in OX5 GSC. Data from 3 biologically independent experiments. One-way Anova analysis represents statistical significance in OX5 GSC treated with DMSO, 415nm, 5-ALA vs. PDT 390 J/cm2/5-ALA at indicated time points (***p < 0.0001), followed by Tukey's post-hoc analysis (***P < 0.0001), error bars represent +/-SD in 3 independent experiments- **(Fig. 22). Img. 10-** Representative image of OX5 GSC 80 min post-PDT/5-ALA taken using Zeiss Microscope (Leica Microsystem, Germany) at 40x.

TUKEY'S HSD	Adjusted P Value
DMSO vs. 5-ALA 100 µM	>0.9999
DMSO vs. 415 nm	>0.9999
DMSO vs. PDT/5-ALA-20 min	0.0027
DMSO vs. PDT/5-ALA-40 min	<0.0001
DMSO vs. PDT/5-ALA-60 min	<0.0001
DMSO vs. PDT/5-ALA-80 min	<0.0001

- The activation of the necroptosis pathway, indicated by p- MLKL at Serine 345, post-PDT/5-ALA treatment in OX5 GSC, excludes the occurrence of apoptotic death events.

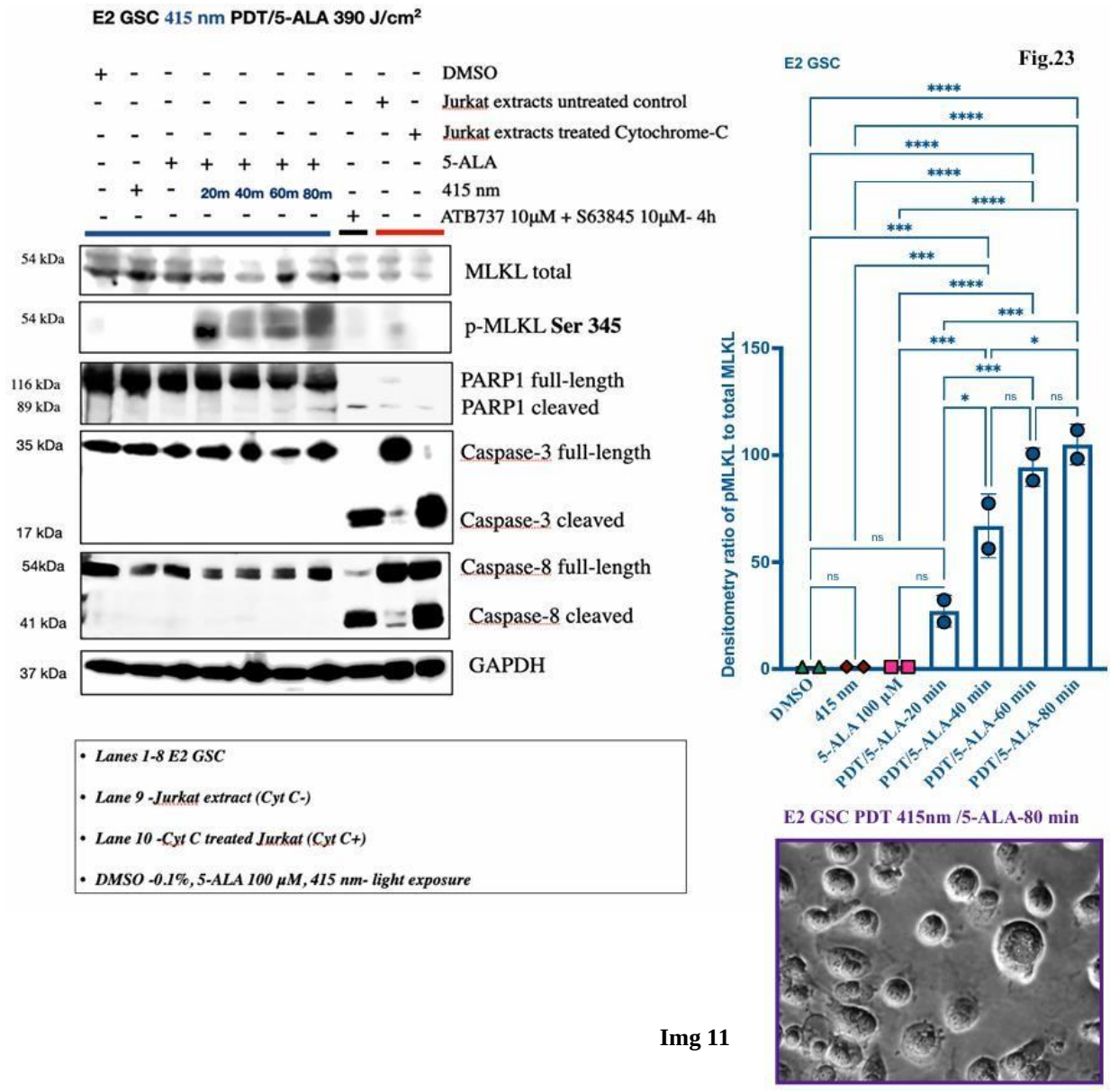

Img 11

WB images represent Necroptosis pathway activation in E2 GSC. Data from 2 biologically independent experiments. One-way Anova analysis represents statistical significance in E2 GSC treated with DMSO, 415nm, 5-ALA vs. PDT 390 J/cm2/5-ALA at indicated time points (***p < 0.0001), followed by Tukey's post-hoc analysis (***P < 0.0001), error bars represent +/-SD in 2 independent experiments- **(Fig. 23). Img. 11-** Representative image of E2 GSC 80 min post PDT/5-ALA taken using Zeiss Microscope (Leica Microsystem, Germany) at 40x.

TUKEY'S HSD	Adjusted P Value
DMSO vs. 5-ALA 100 µM	>0.9999
DMSO vs. 415 nm	>0.9999
DMSO vs. PDT/5-ALA-20 min	0.1145
DMSO vs. PDT/5-ALA-40 min	0.0008
DMSO vs. PDT/5-ALA-60 min	<0.0001
DMSO vs. PDT/5-ALA-80 min	<0.0001

- The presence of p-MLKL at Serine 345, observed following PDT/5-ALA treatment in E2 GSC, signifies the activation of the necroptosis pathway, thereby precluding the involvement of apoptotic death events.

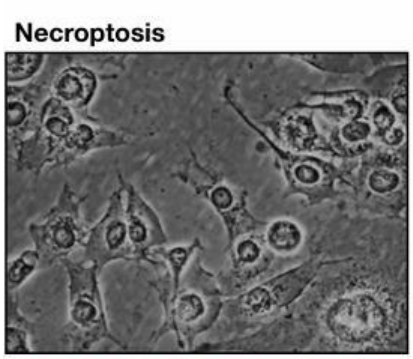

Img.12

G7 GSC PDT 390J/cm^2 415 nm/5-ALA 80 min after exposure

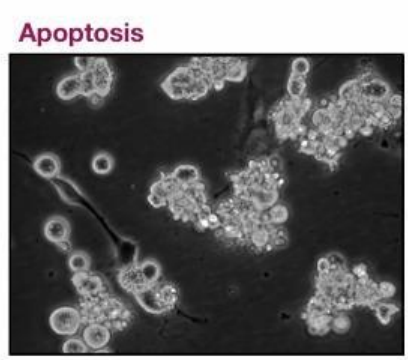

Img.13

G7 GSC treated ATB737 & S63845 for 4 h

The subsequent morphological comparison between G7 GSC post-PDT/5-ALA treatment, indicating activation of the Necroptosis pathway **(Img. 12),** and those subjected to BH-3 mimetics targeting BCL-2, and MCL-1 inhibitors, showcasing apoptotic death events **(Img. 13),** elucidates the primary distinctions. Representative images of G7 GSCs were captured utilising a Zeiss Microscope (Leica Microsystem, Germany) at 40x magnification.

Here, it was provided the main differences between two cell death mechanisms. Necroptosis is characterised by cellular swelling and rupture, releasing contents into the extracellular space, while apoptosis entails cell shrinkage and fragmentation without membrane rupture. Necroptotic cells may experience compromised membrane integrity and display swollen nuclei, whereas apoptotic cells exhibit fragmented nuclei. Necroptosis triggers an inflammatory response (via mediated-pyroptosis cell death) through the release of danger signals, contrasting with the immunological silence of apoptosis.

The activation of the necroptosis pathway post-PDT/5-ALA and the resistance of apoptotic death events lead to the activation of mediated cell death such as parthanatos **[**33**]**. To investigate this phenomenon, experiments were employed to determine whether Apoptosis-inducing factor (AIF), residing in mitochondria, translocates to nuclei, causing caspase-independent DNA damage following PDT/5-ALA treatment.

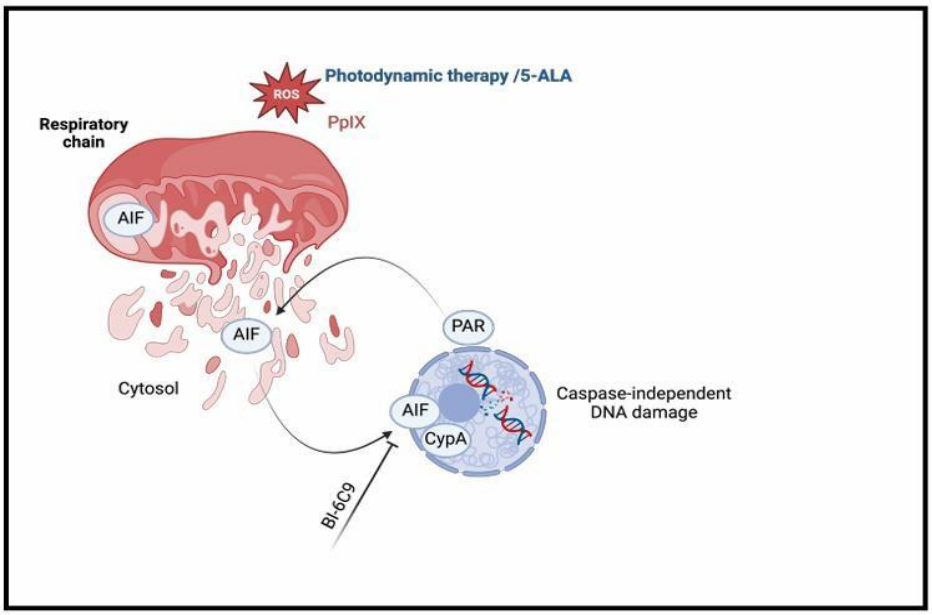

Img.14

Licence- https://app.biorender.com/illustrations/65cde4eb10cfa696f4157436

This schematic illustration succinctly portrays the sequential events triggered by PDT/ 5-ALA, culminating in the release of AIF from mitochondria and its involvement as mediated cell death via the parthanatos pathway **(Img. 14).** Excessive accumulation of PAR polymers contributes to mitochondrial dysfunction and further exacerbates oxidative stress, thereby amplifying the cellular damage initiated by PDT/5-ALA. AIF release from mitochondria can act as a trigger for necroptosis in GSCs where caspase- 8 activity is inhibited. Once released into the cytoplasm, AIF can engage with nuclei causing DNA fragmentation independently from caspases.

Among the various forms of immunogenic cell death, pyroptosis and parthanatos emerge as mediated deaths with anti-tumour immunity. My focus lies in investigating parthanatos, a mode of cell death intricately tied to programmed necrosis. This interest stems from its activation pathway, closely linked to necroptosis, notably observed in G7, OX5, and E2 GSCs. Research delves into mediated cell death phenomena, particularly parthanatos, triggered following the activation of the necroptosis pathway. This process induces extensive caspase-independent DNA damage, potentially post-PDT using 5-ALA. Additionally, the activation of parthanatos precludes apoptosis initiation, highlighting the distinctiveness of this cell death pathway. This critical understanding of intricate cellular responses post-PDT/5-ALA administration holds significant implications for devising combinational therapeutic strategies in glioblastoma management, particularly with DNA checkpoint inhibitors in GSCs exhibiting unmethylated status and resistance to classical apoptosis.

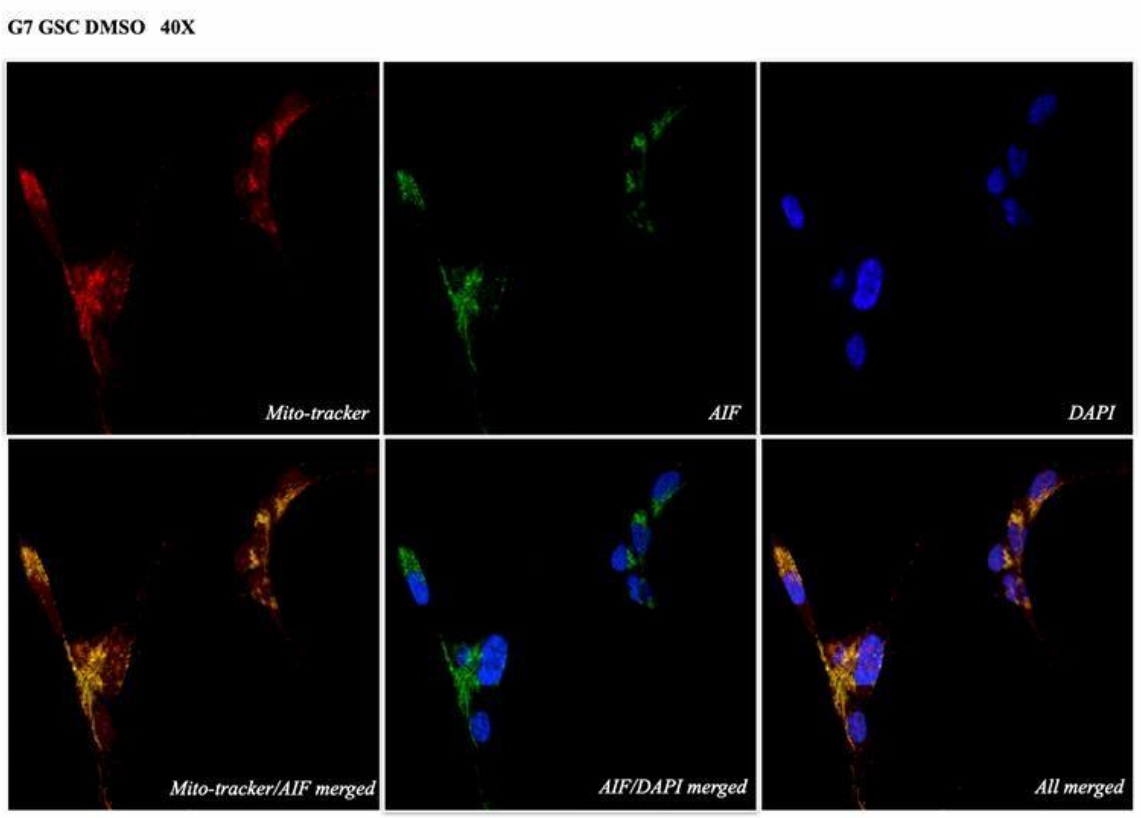

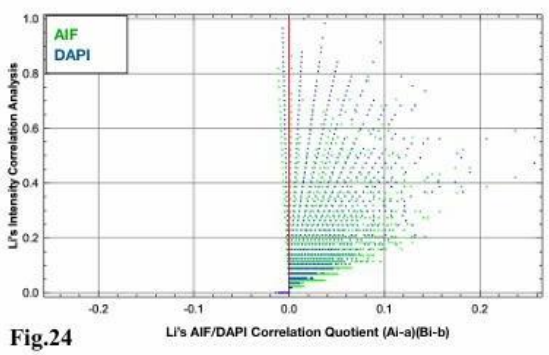

Fig.24

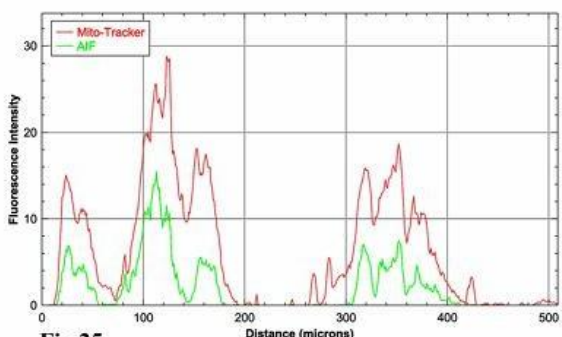

Fig.25

Representative IF images from 2 independent experiments in G7 GSC after DMSO treatment. Pearson's correlation coefficient r=0.873 (AIF/Mito-tracker merged), Mander's coefficient of AIF in Mitochondria M=0.718. Fluorescence intensity analysis depicts that AIF is localised in mitochondria in G7 GSC treated with DMSO control **(Fig. 25).** Pearson's coefficient r=0.118 (AIF /DAPI merged), Mander's coefficient of AIF in Nuclei M=0.162, Li's Correlation Quotient <0.5, therefore, there is no colocalisation between AIF and DAPI.

Cytofluorogram illustrates that AIF is not localised in nuclei in G7 GSC DMSO treated control **(Fig. 24)**

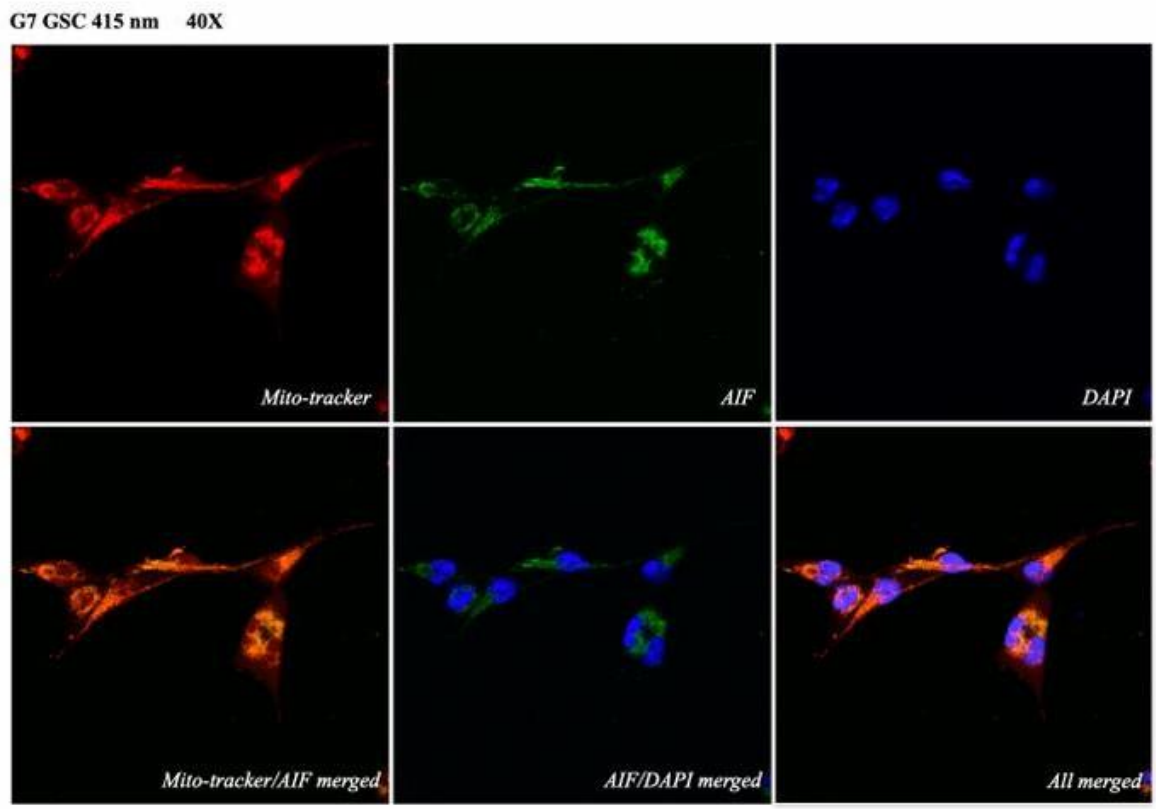

Representative IF images from 2 independent experiments in G7 GSC after 415nm (light only) 390 J/cm2. Pearson's correlation coefficient r=0.807 (AIF/Mito-tracker merged), Mander's coefficient of AIF in Mitochondria M=0.98. Fluorescence intensity analysis demonstrates that AIF is localised within the mitochondria in G7 GSCs treated with 415 nm 390J/cm2 **(Fig. 27).** Pearson's coefficient r=0.2(AIF/DAPI merged), Mander's coefficient of AIF in Nuclei M=0.11, Li's Correlation Quotient <0.5, therefore, there is no colocalisation between AIF and DAPI **(Fig. 26)**. Cytofluorogram analysis shows that AIF is not localised in nuclei in G7 GSC after exposure to the 415 nm 390 J/cm^2 **(Fig. 26).**

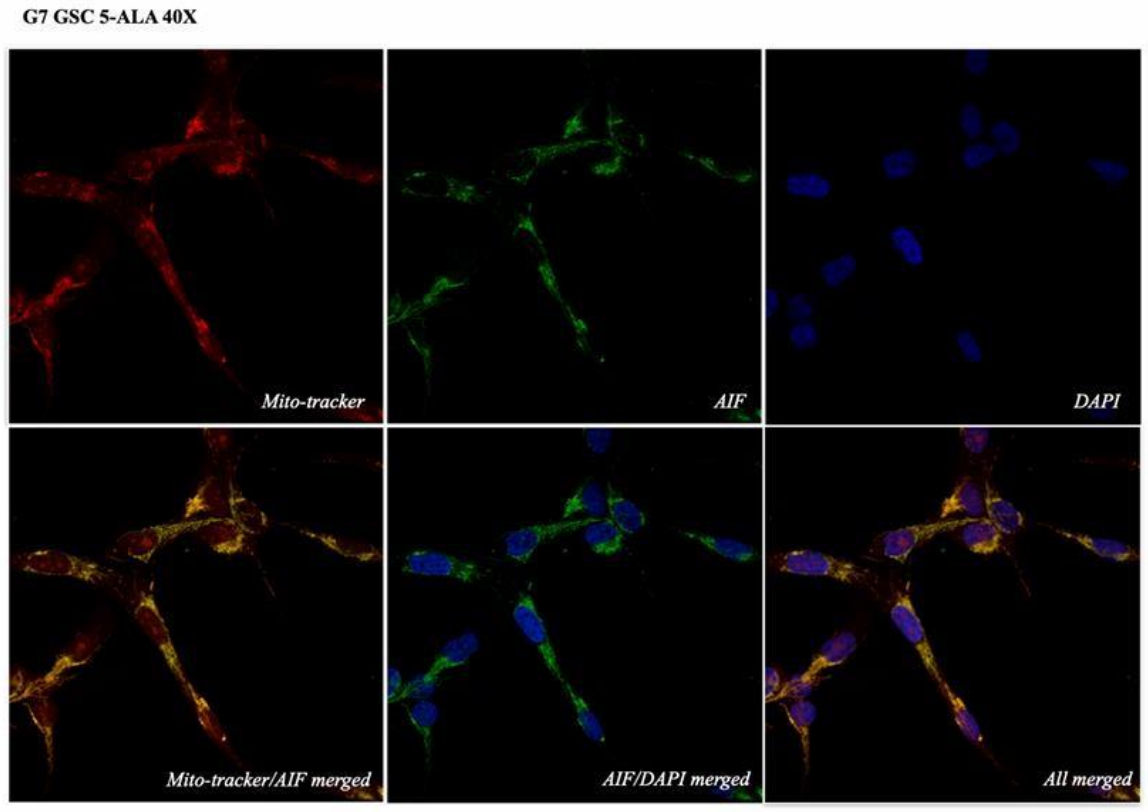

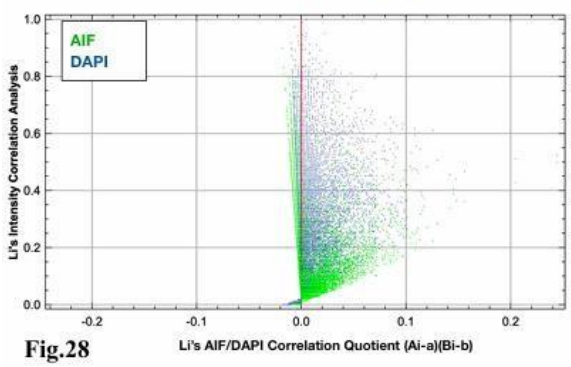

Fig.28

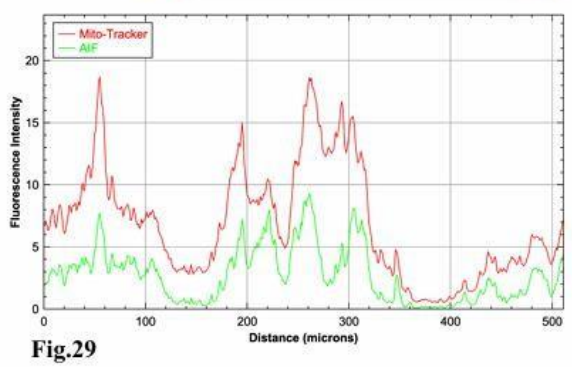

Fig.29

Representative IF images from 2 independent experiments in G7 GSC treated with 5-ALA 100 µM for 3 h. Pearson's correlation coefficient r=0.894-(AIF/Mito-tracker merged), Mander's coefficient of AIF in Mitochondria M=0.991. Fluorescence intensity analysis reveals that AIF is localised within the mitochondria in G7 GSCs treated with 100 µM 5-ALA **(Fig. 29).** Pearson's coefficient r=0.1-(AIF /DAPI merged), Mander's coefficient of AIF in Nuclei M=0.13, Li's Correlation Quotient< 0.5, therefore, there is no colocalisation between AIF and DAPI. Cytofluorogram is shown where AIF is not localised in nuclei in G7 GSC after 5-ALA 100 µM treatment **(Fig.28)**

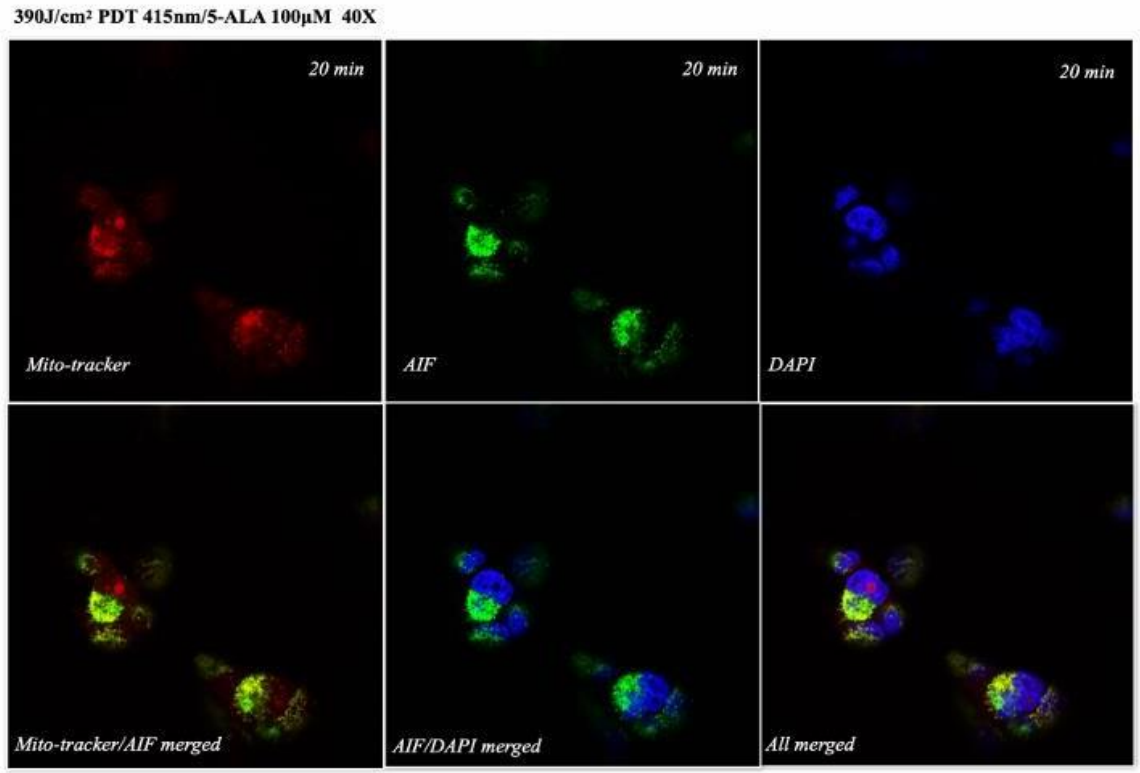

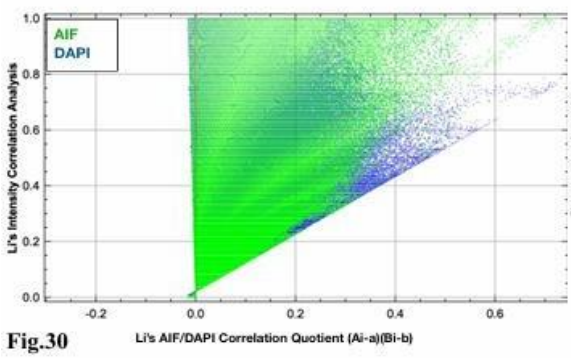

Fig.30

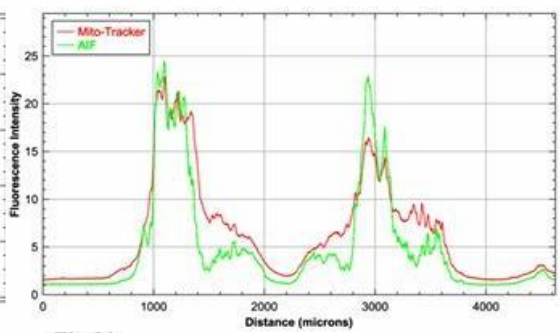

Fig.31

IF images 20 min after PDT/5-ALA (exposure time -16 min, 4s), representatives from 2 independent experiments. G7 GSC illuminated by PDT 390 J/cm2 415nm/5-ALA 100 μM. Pearson's correlation coefficient r=0.845- (AIF/Mito tracker merged), Mander's coefficient of AIF in Mitochondria M=0.71. Fluorescence intensity analysis reveals AIF localisation in mitochondria in G7 GSC 20 min after exposure **(Fig. 31).** Pearson's coefficient r=0.26- (AIF/DAPI merged), Mander's coefficient of AIF in Nuclei M=0.31, Li's Correlation Quotient >0.5, - colocalisation is presented between AIF and DAPI. Cytofluorogram analysis reveals that around 30% of AIF is localised in nuclei in G7 GSC 20 min after illumination **(Fig. 30)**

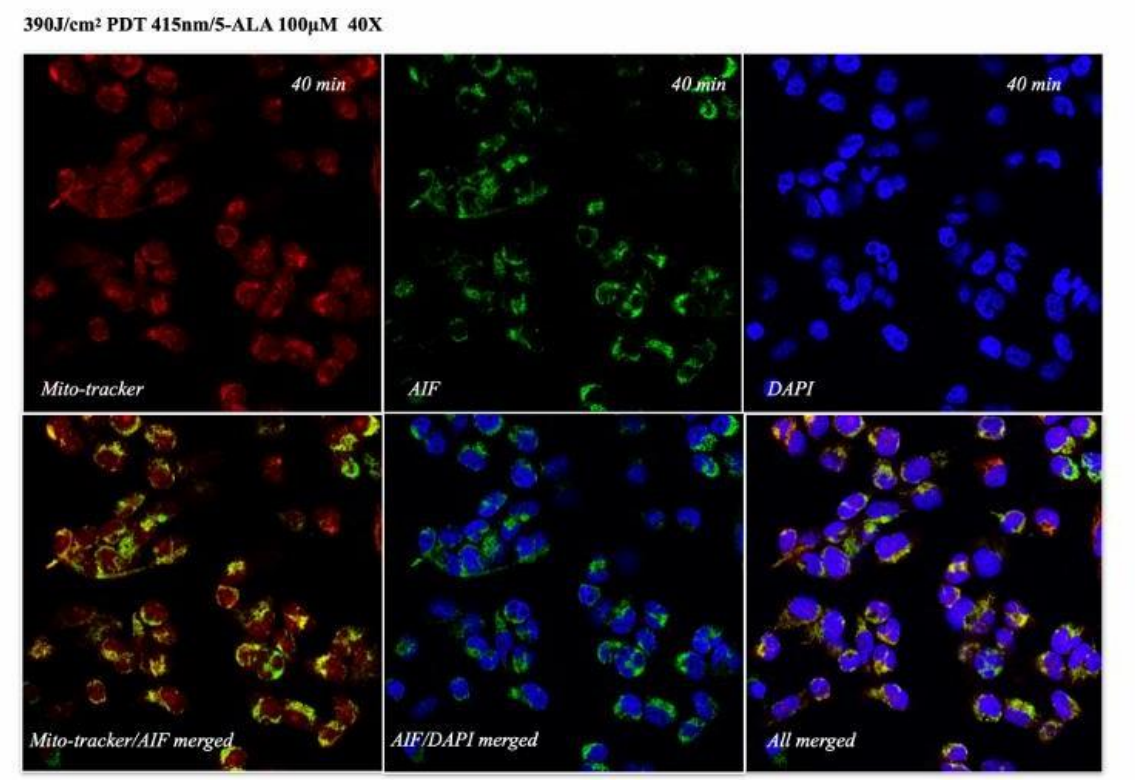

IF images 40 min after exposure to PDT/5- ALA (16 min, 4s), representatives from 2 independent experiments. G7 GSC illuminated by PDT 390 J/cm2 415nm/5-ALA 100 μM. Pearson's correlation coefficient r=0.704-(AIF/Mito-tracker merged), Mander's coefficient of AIF in Mitochondria M=0.723. Fluorescence intensity analysis reveals that around 72% of AIF is localised in mitochondria in G7 GSC 40 min after exposure **(Fig. 33).** Pearson's coefficient r=0.14-(AIF/DAPI merged), Mander's coefficient of AIF in Nuclei M=0.376, Li's Correlation Quotient > 0.5, - colocalisation is presented between AIF and DAPI. Cytofluorogram analysis demonstrates that around 37 % of AIF is localised in nuclei in G7 GSC 40 min after illumination **(Fig. 32)**

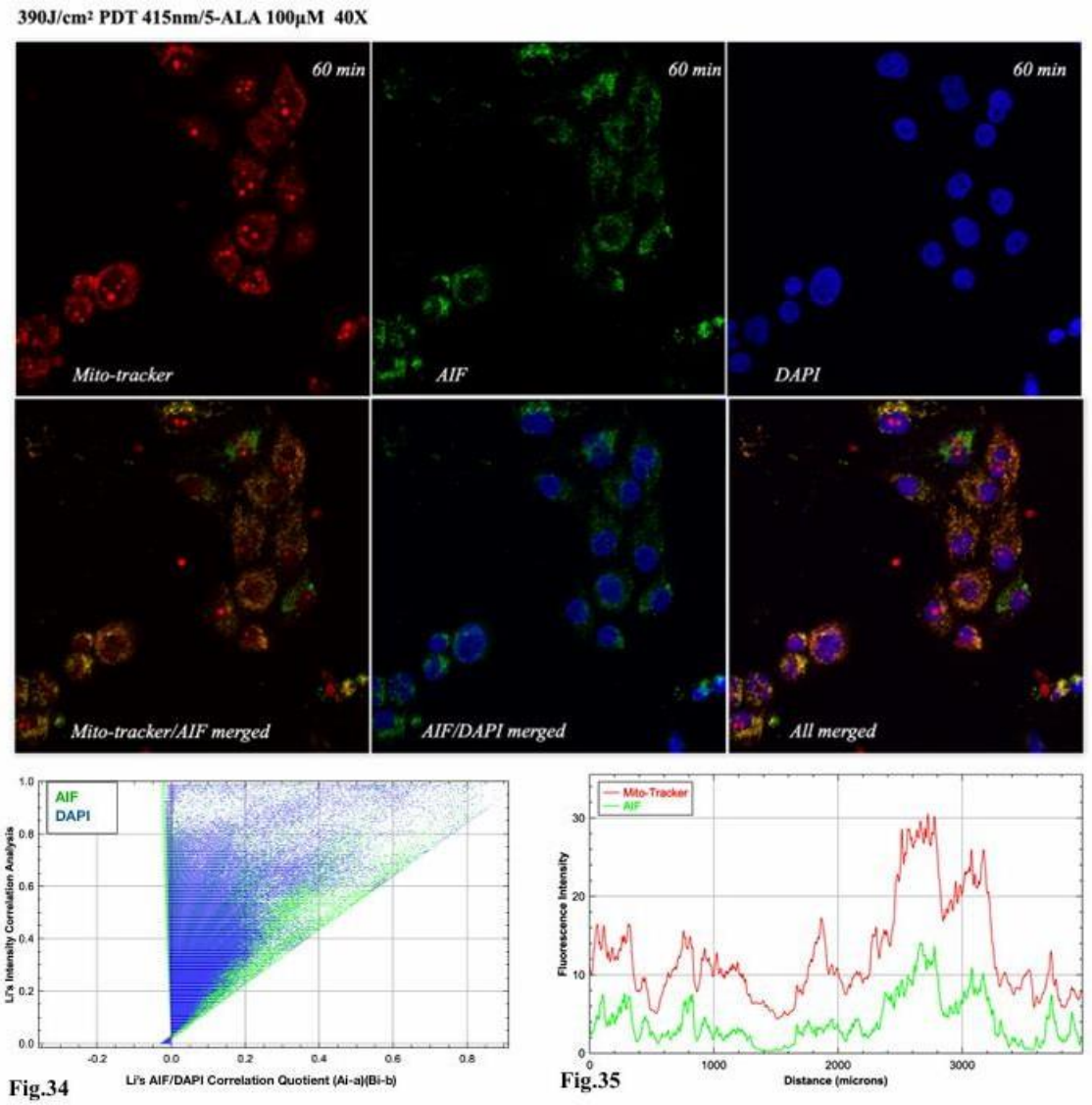

IF images 60 min after exposure to PDT/5-ALA (16 min, 4s), representatives from 2 independent experiments. G7 GSC illuminated by PDT 390 J/cm2 415nm/5-ALA 100 μM. Pearson's correlation coefficient r=0.492-(AIF/Mito-tracker merged), Mander's coefficient of AIF in Mitochondria M=0.493. Fluorescence intensity analysis demonstrates that around 49% of AIF in mitochondria 60 min after illumination **(Fig. 35).** Pearson's coefficient r=0.267-(AIF/DAPI merged), Mander's coefficient of AIF in Nuclei M=0.401, Li's Correlation Quotient >0.5, - colocalisation is presented between AIF and DAPI. Cytofluorogram analysis shows that around 40% of AIF is localised in nuclei in G7 GSC 60 min after illumination **(Fig. 34)**

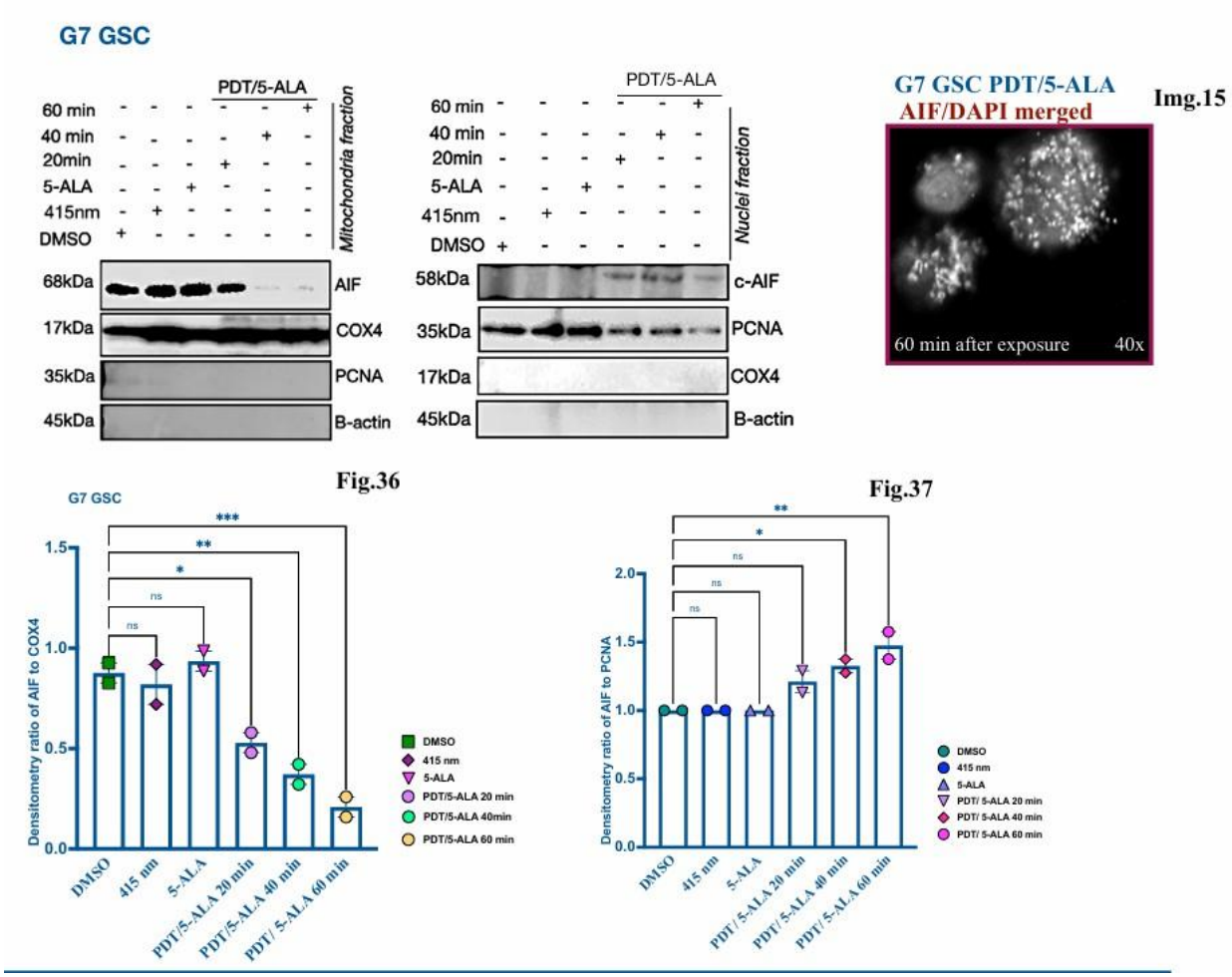

WB in G7 GSC represents 2 biological replicates of nuclei and mitochondrial fractions. Mitochondria fraction demonstrates release of AIF post-PDT/5-ALA in the time dependent manner **-(Fig.36).** One-way Anova analysis was followed by Tukey's test (*** p< 0.0009 -60 min after exposure, ** p< 0.0246- 20 min after exposure). No significance (ns, p> 0.9377, p> 0.9278). Error bars represent+/- SEM. Nuclei fraction demonstrates transition of AIF post-PDT/5-ALA in nuclei **(Fig.37).** One-way Anova analysis followed by Tukey's post-hoc test performed (** p< 0.0035 - 60 min after exposure, * p< 0.0221 - 40 min after exposure). No significance (ns, p>0.9999, p>0.9999, p>0.1201). Error bars represent+/- SEM. **(Img.15)** - Representative black/white image of G7 GSC (AIF&DAPI merged) taken under fluorescent microscope.

The translocation of AIF into the nuclei following PDT/5-ALA treatment **(Fig. 37, Img. 15)** induces 5-ALA PDT/5-ALA 20 min caspase-independent DNA damage in G7 GSCs, intricately linked to the necroptosis death pathway. PDT/5-ALA 40 min This process serves as a mechanism of mediated cell death known as parthanatos.

Discussion

The present study elucidates the critical roles of necroptosis and parthanatos as key cell death pathways activated following PDT with 5-ALA in GSCs. These findings provide significant insights into the molecular mechanisms underlying PDT, establishing a foundation for enhancing its clinical efficacy, particularly in the neurosurgical management of glioblastoma. PDT/5-ALA has been demonstrated to selectively target GSCs at a clinically relevant dose of 160 J/cm², while preserving healthy brain tissue, as modeled by mAS, thereby potentially minimizing adverse effects and enhancing the safety profile of this therapeutic strategy.

Necroptosis as a Targeted Cell Death Mechanism Post-PDT/5-ALA

Necroptosis, a regulated form of necrotic cell death distinct from apoptosis, is characterized by the activation of RIPK1 and RIPK3 and the subsequent phosphorylation of MLKL. The current study demonstrates that PDT/5-ALA effectively induces necroptosis in G7, OX5, and E2 GSCs, as evidenced by MLKL phosphorylation and the inhibition of cell death by NSA, a specific necroptosis inhibitor. The absence of caspase-3 activation further confirms the non-apoptotic nature of cell death induced by PDT. The formation of the necrosome complex, initiated by tumor necrosis factor-alpha (TNF-α) and other death receptor ligands, underscores PDT's specificity in targeting apoptosis-resistant glioma cells. This mechanism is particularly relevant in neurosurgical contexts, where eliminating tumor cells that evade conventional therapies is paramount.

Parthanatos and Mitochondrial Disruption Following PDT/5-ALA

Parthanatos, a distinct form of programmed cell death driven by excessive activation of poly (ADP-ribose) polymerase-1 (PARP-1), complements necroptosis in the cytotoxic response to PDT. ROS generated during PDT induces extensive DNA damage, leading to hyperactivation of PARP-1, which results in NAD+ depletion and subsequent cellular energy failure. This triggers the translocation of AIF from the mitochondria to the nucleus, exacerbating mitochondrial dysfunction in the absence of caspase-8 activity. The study's data reveal that parthanatos is a critical component of the cell death response in G7 GSCs, as indicated by AIF-mediated chromatin condensation and DNA fragmentation. This dual impairment of energy metabolism and mitochondrial integrity underscores the efficacy of PDT in overcoming the

apoptotic resistance often observed in glioblastoma.

Clinical Relevance and Implications for Neurosurgical Practice

These molecular insights have significant implications for clinical practice, particularly in the neurosurgical management of glioblastoma. Although PDT/5-ALA is effective in targeting GSCs within 0.5 cm of the surgical cavity, its limited depth of penetration leaves deeper tumor cells, up to 2.5 cm from the resection margin, untreated. The findings suggest that combining PDT/5-ALA with small-molecule inhibitors targeting apoptosis regulators, such as the BCL-2 family (ATB737 and S63845), could overcome these limitations by sensitizing tumor cells to apoptosis, thereby extending the therapeutic reach of PDT.

Strategic Integration of PDT with Immunotherapy

The activation of necroptosis and parthanatos not only ensures the eradication of tumor cells but also has the potential to elicit an immunogenic response due to the release of DAMPs during necroptosis. This immunogenic cell death presents a strategic opportunity to combine PDT with immunotherapy. Coupling PDT-induced cell death with immune checkpoint inhibitors or other immunomodulatory therapies could amplify the immune-mediated clearance of glioblastoma cells, including those beyond the direct reach of PDT. Such an approach could transform PDT from a predominantly local treatment modality into a central component of a multimodal therapeutic strategy for glioblastoma.

Conclusion

In summary, the activation of necroptosis and parthanatos following PDT/5-ALA underscores the utility of these non-apoptotic pathways in targeting apoptosis-resistant GSCs. The proposed combination of PDT with immunotherapy and apoptosis-sensitizing agents holds significant promise for enhancing therapeutic outcomes in glioblastoma treatment, particularly in the context of neurosurgical resection and clinical trials. This integrative approach might offers a more comprehensive and effective strategy for managing this highly aggressive malignancy, ultimately improving patient prognosis.

Conflict of Interest Statement

The authors declare no conflicts of interest related to this research. * Nazar Vasyliv is the CEO of the Global Alliance for Neurosurgical & Brain Cancer Research Innovations, a role that has not influenced the design, conduct, or reporting of this study. No financial or personal relationships could affect the research outcomes.

Research Ethics Statement

This study was conducted in compliance with ethical standards set by the Research Integrity University of Edinburgh. Ethical approval was granted by the University's Research Ethics Committee, and all procedures involving human participants adhered to institutional and national regulations. Informed consent was obtained from all participants, and their privacy was strictly maintained.

Video Presentation: https://files.ukr.net/get/26nmgtpk2s:589514093/Global Alliance video.mov

Reference

1. Stupp, R., Mason, W. P., van den Bent, M. J., Weller, M., Fisher, B., Taphoorn, M. J., ... & Mirimanoff, R. O. (2005). Radiotherapy plus concomitant and adjuvant temozolomide for glioblastoma. New England Journal of Medicine, 352(10), 987-996.
2. Weller, M., Cloughesy, T., Perry, J. R., & Wick, W. (2013). Standards of care for treatment of recurrent glioblastoma—are we there yet? Neuro-oncology, 15(1), 4-27.
3. Sanai, N., Polley, M. Y., McDermott, M. W., Parsa, A. T., & Berger, M. S. (2011). An extent of resection threshold for newly diagnosed glioblastomas. Journal of Neurosurgery, 115(1), 3-8.
4. Stummer, W., Novotny, A., Stepp, H., Goetz, C., Bise, K., & Reulen, H. J. (2000). Fluorescence-guided resection of glioblastoma multiforme by using 5-aminolevulinic acid–induced porphyrins: a prospective study in 52 consecutive patients. Journal of Neurosurgery, 93(6), 1003-1013.
5. Krammer, B. (2001). Vascular effects of photodynamic therapy. Anticancer Research, 21(6B), 4271-4277.
6. Kaiser, J. C., & Attardi, L. D. (2018). Deconstructing networks of p53-mediated tumor suppression in vivo. Cell Death and Differentiation, 25(1), 93-103.

7. Sanai, N., & Berger, M. S. (2008). Glioma extent of resection and its impact on patient outcome. Neurosurgery, 62(4), 753-766.

8. Lacroix, M., Abi-Said, D., Fourney, D. R., Gokaslan, Z. L., Shi, W., DeMonte, F., ... & Sawaya, R. (2001). A multivariate analysis of 416 patients with glioblastoma multiforme: prognosis, extent of resection, and survival. Journal of Neurosurgery, 95(2), 190-198.

9. Stummer, W., Tonn, J. C., Mehdorn, H. M., Nestler, U., Franz, K., Goetz, C., ... & Reulen, H. J. (2006). ALA-Glioma Study Group. Journal of Neurosurgery, 105(1), 6-12.

10. Stummer, W., & Kamp, M. A. (2009). The importance of surgical resection in malignant glioma. Current Opinion in Neurology, 22(6), 645-649.

11. Van Tellingen, O., Yetkin-Arik, B., de Gooijer, M. C., Wesseling, P., Wurdinger, T., & de Vries, H. E. (2015). Overcoming the blood–brain tumor barrier for effective glioblastoma treatment. Drug Resistance Updates, 19, 1-12.

12. Huang, Z. (2005). A review of progress in clinical photodynamic therapy. Technology in Cancer Research & Treatment, 4(3), 283-293.

13. Krysko, D. V., Garg, A. D., Kaczmarek, A., Krysko, O., Agostinis, P., & Vandenabeele, P. (2012). Immunogenic cell death and DAMPs in cancer therapy. Nature Reviews Cancer, 12(12), 860-875.

14. Agostinis, P., Berg, K., Cengel, K. A., Foster, T. H., Girotti, A. W., Gollnick, S. O., ... & Kessel, D. (2011). Photodynamic therapy of cancer: an update. CA: A Cancer Journal for Clinicians, 61(4), 250-281.

15. Hamblin, M. R., & Mroz, P. (Eds.). (2008). Advances in photodynamic therapy: basic, translational, and clinical. Artech House.

16. Galluzzi, L., Kepp, O., & Kroemer, G. (2012). Enlightening the impact of immunogenic cell death in photodynamic cancer therapy. EMBO Journal, 31(5), 1055-1057.

17. Vandenabeele, P., Galluzzi, L., Vanden Berghe, T., & Kroemer, G. (2010). Molecular mechanisms of necroptosis: an ordered cellular explosion. Nature Reviews Molecular Cell Biology, 11(10), 700-714.

18. Pasparakis, M., & Vandenabeele, P. (2015). Necroptosis and its role in inflammation. Nature, 517(7534), 311-320.

19. Fulda, S. (2015). Targeting apoptosis signaling pathways for anticancer therapy. Frontiers in Oncology, 5, 120.

20. Najafov, A., Chen, H., Yuan, J. (2017). Necroptosis and cancer. Trends in Cancer, 3(4), 263-269.

21. Tait, S. W., & Green, D. R. (2010). Mitochondria and cell signalling. Journal of Cell Science, 123(6), 807-812.

22. Housley, M. P., Udeshi, N. D., Rodgers, J. T., Shabanowitz, J., Puigserver, P., Hunt, D. F., & Hart, G. W. (2009). A PGC-1α–O-GlcNAc transferase complex regulates FoxO transcription factor activity in response to glucose. Journal of Biological Chemistry, 284(8), 5148-5157.

23. Stummer, W., Pichlmeier, U., Meinel, T., Wiestler, O. D., Zanella, F., & Reulen, H. J. (2006). Fluorescence-guided surgery with 5-aminolevulinic acid for resection of malignant glioma: a randomised controlled multicentre phase III trial. Lancet Oncology, 7(5), 392-401.

24. Stummer, W., Pichlmeier, U., Meinel, T., Wiestler, O. D., Zanella, F., & Reulen, H. J. (2006). Fluorescence-guided surgery with 5-aminolevulinic acid for resection of malignant glioma: a randomised controlled multicentre phase III trial. Lancet Oncology, 7(5), 392-401.

25. Agostinis, P., Berg, K., Cengel, K. A., Foster, T. H., Girotti, A. W., Gollnick, S. O., Kessel, D. (2011). Photodynamic therapy of cancer: an update. *CA: A Cancer Journal for Clinicians*, 61(4), 250-281.

26. Galluzzi, L., Vitale, I., Abrams, J. M., Alnemri, E. S., Baehrecke, E. H., Blagosklonny, M. V., ... & Kroemer, G. (2018). Molecular mechanisms of cell death: recommendations of the Nomenclature Committee on Cell Death 2018. Cell Death & Differentiation, 25(3), 486-541.

27. Shibata, A., & Ueno, M. (2017). Targeted therapies and immunotherapies for glioblastoma: clinical trials update and future perspectives. Current Oncology Reports, 19(7), 53.

28. Tanaka, R., Kumabe, T., Yoshimoto, T., & Nakazato, Y. (1995). Glioblastoma multiforme in an elderly population. Journal of Neuro-Oncology, 23(1), 29-36.

29. Stupp, R., Mason, W. P., van den Bent, M. J., Weller, M., Fisher, B., Taphoorn, M. J., ... & Mirimanoff, R. O. (2005). Radiotherapy plus concomitant and adjuvant temozolomide for glioblastoma. New England Journal of Medicine, 352(10), 987-996.

30. Clarke, J., Butowski, N., & Chang, S. (2010). Recent advances in therapy for glioblastoma. Archives of Neurology, 67(3), 279-283.

31. Finsen, N. R. (1904). Phototherapy: Nobel Lecture. The Nobel Prize Foundation.

32. Von Tappeiner, H., & Jesionek, A. (1903). Therapeutic activity of fluorescent substances. Dermatologische Zeitschrift, 10, 179-186.

33. Dougherty, T. J. (1993). Photodynamic therapy. Photochemistry and Photobiology, 58(6), 895-900.

34. Dolmans, D. E., Fukumura, D., & Jain, R. K. (2003). Photodynamic therapy for cancer. Nature Reviews Cancer, 3(5), 380-387.

35. Fayter, D., Corbett, M., Heirs, M., Fox, D., Eastwood, A., & Payne, E. (2010). A systematic review of photodynamic therapy in the treatment of pre-cancerous skin conditions, Barrett's esophagus and cancers of the biliary tract, brain, head and neck, lung, esophagus and soft tissues. Health Technology Assessment, 14(37), 1-288.

36. Henderson, B. W., & Dougherty, T. J. (1992). How does photodynamic therapy work? Photochemistry and Photobiology, 55(1), 145-157.

37. Allison, R. R., Moghissi, K., Downie, G. H., & Dixon, K. (2011). Photodynamic therapy (PDT) for lung cancer. Photodiagnosis and Photodynamic Therapy, 8(3), 231-239.

38. Agostinis, P., Berg, K., Cengel, K. A., Foster, T. H., Girotti, A. W., Gollnick, S. O., ... & Kessel, D. (2011). Photodynamic therapy of cancer: an update. CA: A Cancer Journal for Clinicians, 61(4), 250-281.

39. Celli, J. P., Spring, B. Q., Rizvi, I., Evans, C. L., Samkoe, K. S., Verma, S., ... & Hasan, T. (2010). Imaging and photodynamic therapy: mechanisms, monitoring, and optimization. Chemical Reviews, 110(5), 2795-2838.

Medtronic